

MEASUREMENT OF WALL SHEAR AND WALL PRESSURE
DOWNSTREAM OF A
HONEYCOMB BOUNDARY LAYER MANIPULATOR

by

JAMES CHRISTIAN MOLLER and PATRICK LEEHEY

Report No. 97457-3

April, 1989

This research was carried out under the Underwater Acoustics Program
Code 1125OA of the Office of Naval Research under contract number
N00014-86-K-0183 .

Approved for public release ; distribution unlimited

Acoustics and Vibration Laboratory

AD-A208 297

DTIC
ELECTE
MAY 3 1 1989
S H D

UNCLASSIFIED

SECURITY CLASSIFICATION OF THIS PAGE (When Data Entered)

REPORT DOCUMENTATION PAGE		READ INSTRUCTIONS BEFORE COMPLETING FORM
1. REPORT NUMBER Acoustics & Vibration Laboratory Report No. 97457-3	2. GOVT ACCESSION NO.	3. RECIPIENT'S CATALOG NUMBER
4. TITLE (and Subtitle) Measurement of Wall Shear and Wall Pressure Downstream of a Honeycomb Boundary Layer Manipulator		5. TYPE OF REPORT & PERIOD COVERED Technical
		6. PERFORMING ORG. REPORT NUMBER
7. AUTHOR(s) James Christian Moller and Patrick Leehey		8. CONTRACT OR GRANT NUMBER(s) N00014-86-R-0183
9. PERFORMING ORGANIZATION NAME AND ADDRESS Massachusetts Institute of Technology Room 2-262 Cambridge, MA 02139		10. PROGRAM ELEMENT, PROJECT, TASK AREA & WORK UNIT NUMBERS ONR Code 11250A
11. CONTROLLING OFFICE NAME AND ADDRESS Office of Naval Research Code 1125 OA Ballston Tower #1 800 N. Quincy St., Arlington, VA 22215-5000		12. REPORT DATE April 1989
		13. NUMBER OF PAGES 73
14. MONITORING AGENCY NAME & ADDRESS (if different from Controlling Office)		15. SECURITY CLASS. (of this report) Unclassified
		15a. DECLASSIFICATION/DOWNGRADING SCHEDULE
16. DISTRIBUTION STATEMENT (of this Report) Approved for public release; distribution unlimited.		
17. DISTRIBUTION STATEMENT (of the abstract entered in Block 20, if different from Report)		
18. SUPPLEMENTARY NOTES		
19. KEY WORDS (Continue on reverse side if necessary and identify by block number) Wall shear stress Wall pressure fluctuations Turbulent boundary layer manipulation		
20. ABSTRACT (Continue on reverse side if necessary and identify by block number) See page 2 of this report.		

DD FORM 1473 1 JAN 73

EDITION OF 1 NOV 65 IS OBSOLETE

UNCLASSIFIED

SECURITY CLASSIFICATION OF THIS PAGE (When Data Entered)

89 5 31 038

MEASUREMENT OF WALL SHEAR AND WALL PRESSURE
DOWNSTREAM OF A
HONEYCOMB BOUNDARY LAYER MANIPULATOR

by

JAMES CHRISTIAN MOLLER and PATRICK LEEHEY

Report No. 97457-3

April, 1989

This research was carried out under the Underwater Acoustics Program
Code 1125OA of the Office of Naval Research under contract number
N00014-86-K-0183 .

Approved for public release ; distribution unlimited

ACOUSTICS AND VIBRATION LABORATORY

Massachusetts Institute of Technology

Cambridge, Massachusetts 02139

MEASUREMENT OF WALL SHEAR AND WALL PRESSURE
DOWNSTREAM OF A
HONEYCOMB BOUNDARY LAYER MANIPULATOR

by

James Christian Moller and Patrick Lechey

ABSTRACT

A boundary layer manipulator in the shape of a honeycomb placed in a turbulent boundary layer has been shown experimentally to reduce local wall shear downstream by as much as 38% and wall pressure by 36%. The zone of measureable shear and pressure reduction extends for at least 300 pre-manipulator displacement thicknesses downstream. Pressure spectra of the manipulated flow scales better with inner-outer variables than does the unmanipulated flow. Convective pressure speeds are reduced by as much as approximately 30% for Strouhal numbers ($\omega\delta^*/U_\infty$) above 0.3. Below $\omega\delta^*/U_\infty = 0.3$ convective phase speeds are not noticeably changed. This indicates pressure disturbances for $\omega\delta^*/U_\infty < 0.3$ may originate from the inner portion of the boundary layer since the manipulator scales are far larger than the viscous sublayer. Coherence appears to be reduced in the streamwise direction and increased in the spanwise direction.

All tests were done in the same facility as in Blake [1] using the same microphones and wall insert. Unlike his work and similar to the work of other more recent investigations [2,3,4], peaks were found in plots of coherence vs. phase in the vicinity of $\omega\delta^*/U_{cp} \approx 0.3$.



Accession For	
NTIS GRA&I	<input checked="" type="checkbox"/>
DTIC TAB	<input type="checkbox"/>
Unannounced	<input type="checkbox"/>
Justification	
By	
Distribution/	
Availability Codes	
Dist	Avail and/or Special
A-1	

ACKNOWLEDGEMENTS

The senior author's tuition and stipend have been largely paid for by a Graduate Fellowship from the National Science Foundation. Other funding was provided by the Office of Naval Research Code 1125OA and the David Taylor Research Center.

TABLE OF CONTENTS

	Page
List of Figures	5
Nomenclature	7
1. Introduction	9
1.1 Background	9
1.2 Objectives	11
2. Experiment Description	11
2.1 The Device	11
2.2 Wind Tunnel	13
2.3 Pressure Measurements	14
2.4 Velocity Measurements	14
2.5 Shear Measurements	15
2.6 Spectral Measurements	16
3. Experimental Results	17
3.1 Mean Velocity	17
3.2 Turbulence Levels	19
3.3 Wall Pressure	19
3.3.1 Point Spectra	19
3.3.2 Streamwise Coherence	20
3.3.3 Spanwise Coherence	21
3.4 Convective Velocities	21
4. Conclusions	22
References	23
Figures	25

LIST OF FIGURES

Figure Number & Title	Page
1a. Honeycomb Manipulator Sketch.	25
1b. Honeycomb Manipulator Photo.	26
2. Wind Tunnel Facility.	27
3. Point Spectra & Shear Measuring Insert.	28
4. Cross-Spectral Insert and Test Section.	28
5. Hot Wire Traverse.	29
6. Surface Fence Wall Shear Stress Gage.	30
7. \bar{u}/U_∞ vs. y/δ^* . Equilibrium Flow.	31
8. u^+ vs. y^+ . Equilibrium Flow.	32
9. \bar{u}/U_∞ vs. y/δ^* . Manipulated Flow. Stations 1,2,3.	33
10. \bar{u}/U_∞ vs. y/h_c . Manipulated Flow. Stations 1,2,3.	36
11. u^+ vs. y^+ . Manipulated Flow. Stations 1,2,3.	39
12. C_f vs. Re_B . Equilibrium, Manipulated, and Empirical Results of Others.	42
13. C_f vs. $\Delta x/\delta^*$ <i>incid</i>	43
14. τ_w vs. Fence differential pressure.	44
15. u'/u^* vs. y/δ^* . Equilibrium Flow.	45
16. u'/u^* vs. y/δ^* . Manipulated Flow. Stations 1,2,3.	46
17. u'/u^* vs. y/h_c . Manipulated Flow. Stations 1,2,3.	49
18. $\sqrt{p'^2/q}$ vs. $\Delta x/\delta^*$ <i>incid</i>	52
19. Point Pressure Spectra. Equilibrium Flow. Outer-Inner Variables.	53
20. Point Pressure Spectra. Manipulated Flow. Outer-Inner Variables.	54
21. Point Pressure Spectra. Equilibrium Flow. Transducer Variables.	57
22. Point Pressure Spectra. Manipulated Flow. Transducer Variables.	58
23. Streamwise Coherence vs. Phase. $r_1/\delta^* = .91, 1.05$	61
24. Streamwise Coherence vs. Phase. $r_1/\delta^* = 2.19, 2.53$	62

25. Streamwise Coherence vs. Phase. $r_1/\delta^* = 4.01, 4.63$	63
26. Streamwise Coherence vs. Phase. $r_1/\delta^* = 6.93, 8.00$	64
27. Streamwise Coherence vs. Phase. $r_1/\delta^* = 11.67, 13.48$	65
28. Spanwise Coherence vs. Phase. $r_3/\delta^* = .91, 1.05$	66
29. Spanwise Coherence vs. Phase. $r_3/\delta^* = 2.19, 2.53$	67
30. Spanwise Coherence vs. Phase. $r_3/\delta^* = 4.01, 4.63$	68
31. Convective Phase Speed vs. Strouhal Number. $r_1/\delta^* = .91, 1.05$	69
32. Convective Phase Speed vs. Strouhal Number. $r_1/\delta^* = 2.19, 2.53$	70
33. Convective Phase Speed vs. Strouhal Number. $r_1/\delta^* = 4.01, 4.63$	71
34. Convective Phase Speed vs. Strouhal Number. $r_1/\delta^* = 6.93, 8.00$	72
35. Convective Phase Speed vs. Strouhal Number. $r_1/\delta^* = 11.67, 13.48$	73

NOMENCLATURE OF SYMBOLS

C_1	Von Karman slope
C_2	Y-intercept of log layer equation
C_f	Friction coefficient
d_c	Mean comb diameter
d^+	Diameter in viscous units, $\frac{du^*}{\nu}$
D	Transducer diameter
h_c	Comb Height
i	$\sqrt{-1}$
<i>incid</i>	Subscript for incident upon manipulator
l	Counting variable in time space
m	Counting variable in frequency space
N	Total number of samples in discrete time series
p	Pressure
P_m	Discrete Fourier Transform of pressure signal
q	Dynamic head, $\frac{\rho U_\infty^2}{2}$
\vec{r}	Separation vector
r_1	Streamwise separation
r_3	Spanwise separation
R_{11}	Autocorrelation function
R_{12}	Crosscorrelation function
Re_δ	Reynolds number based on displacement thickness
Re_x	Reynolds number based on distance from contraction
u	Fluctuating streamwise component of velocity
\bar{u}	Mean velocity, streamwise direction

u^*	Friction velocity, $\sqrt{\frac{\tau_w}{\rho}}$
u'	Root mean squared value of fluctuating velocity
u^+	$\frac{\bar{u}}{u^*}$
U	Total streamwise component of velocity
U_{cp}	Convective phase velocity
U_∞	Free stream velocity
v	Fluctuating spanwise component of velocity
x	Distance from end of contraction
Δx	Distance from exit of honeycomb to measuring station
y	Distance from wall to measuring point
y^+	Distance from wall in viscous units, $\frac{y u^*}{\nu}$
$\alpha(r_1, \omega)$	Phase of cross-spectral density
δ^*	Displacement thickness
$\Gamma(\omega, r)$	Coherence
λ	Taylor microscale
μ	Fluid viscosity
ν	Fluid kinematic viscosity
ω	Radian frequency
$\Phi(\omega)$	Pressure spectral density
$\Phi(r_1, 0, \omega)$	Streamwise cross-spectral density
$\Phi(0, r_3, \omega)$	Spanwise cross-spectral density
ρ	Fluid density
τ	Variable of time integration or time delay between signals
τ_w	Mean wall shear stress

1. INTRODUCTION

1.1. Background

The use of devices to alter and control the structure of turbulent boundary layers, most notably the Large Eddy Breakup Device (or LEBU), have been studied by several researchers in recent years. The primary goal of this research has been to investigate the viability of the LEBU as a drag reduction device. While an understanding of the flow behavior around a LEBU is reasonably well understood, results have been mixed and seem to differ because of differences in test facilities [5]. While some have achieved an overall (plate plus device) drag reduction, others with seemingly similar experimental rigs have not gotten the same results. The idea of manipulating the boundary layer is still a viable one, however, from the standpoint of wall pressure reduction because manipulators do create local (but not overall) reductions in wall shear for many boundary layers downstream. Knowledge of boundary layer wall pressure spectra and the means of controlling it have several aero- and hydro-acoustic applications. Perhaps the foremost areas are for the prediction and control of flow-induced vibration and the control of boundary layer self noise over a hydrophone array. Beeler [6] has reported net reductions of wall pressure of 12.5% downstream of a tandem LEBU. The gains to be had from boundary layer control can be significant. For example, detection probability by a submarine can conceivably be increased 40% by a 10 db increase in signal-to-noise ratio [7].

The linkage between wall shear and wall shear pressure is as follows. It is hypothesized wall pressure scales with mean wall shear stress. If we begin with the Navier-Stokes and continuity equations,

$$\frac{D\vec{U}}{Dt} = \frac{-1}{\rho} \nabla p + \nu \nabla^2 \vec{U}$$

and

1. Blake, W. K., (1970), "Turbulent boundary-layer wall-pressure fluctuations on smooth and rough walls", J. Fluid Mechanics, vol. 44, part 4, pp. 637-660.
2. Farabee, Theodore M., (1986), "An Experimental Investigation of Wall Pressure Fluctuations Beneath Non-Equilibrium Flows", D. W. Taylor Naval Ship R & D Center, Rept. No. DTNSRDC-86/047, pg. 126, (May 1986)
3. Brooks, T.F. and Hodgson, T.H., (1981), "Trailing Edge Noise Prediction From Measures Surface Pressures", J. Sound and Vibration, vol. 78, No. 1, pp. 69-117.
4. Narayan, N. and Plunkett, R., (1985), "Pressure Cross Spectra in turbulent Boundary Layers in Water", ASME Winter Annual Mtg., Miami Beach, Fla., Nov. 17-22, NCA-Vol. 1, pp. 97-103.
5. Brown, Eugene F., "European Mtg. on Turbulent Drag Reduction", ESN 41-2, 1987, pg. 89.

$$\nabla \cdot \vec{U} = 0$$

Taking the divergence of both sides gives

$$\nabla \cdot \frac{\partial \vec{U}}{\partial t} + \nabla \cdot (\vec{U} \cdot \nabla) U = -\frac{1}{\rho} \nabla^2 p + \nu \nabla \cdot \nabla^2 \vec{U}$$

where

$$\nabla \cdot (\nabla^2 \vec{U}) = \nabla \cdot [\nabla(\nabla \cdot \vec{U}) - \nabla \times (\nabla \times \vec{U})]$$

The first term on the right hand side is zero due to continuity and the second is zero by the rules of vector algebra. Also by continuity and vector algebra,

$$\nabla \cdot \frac{\partial \vec{U}}{\partial t} = \frac{\partial}{\partial t} \nabla \cdot \vec{U} = 0$$

Which leaves the Poisson equation,

$$\nabla \cdot (\vec{U} \cdot \nabla) \vec{U} + \frac{1}{\rho} \nabla^2 p = 0$$

or

$$\nabla^2 p + \rho \frac{\partial^2 (U_i U_j)}{\partial x_i \partial x_j} = 0$$

After rewriting pressure and velocity in terms of mean and fluctuating quantities and requiring the flow field to have a single nonzero mean vector component, the equation to describe fluctuating pressure in a boundary layer is

$$\nabla^2 p' = -\rho \left[2 \frac{\partial \bar{u}}{\partial y} \frac{\partial v}{\partial x} - \frac{\partial^2 (u_i' u_j' - \overline{u_i' u_j'})}{\partial x_i \partial x_j} \right]$$

The first term inside the bracket is known as the mean shear-turbulence interaction term and has been experimentally found to be the dominant source of pressure fluctuations. In it is a link to wall shear because mean wall shear is linearly related to the mean velocity gradient at the wall. The second part of the mean shear turbulence term, $\partial v / \partial x$, was beyond the scope of this set of experiments but would need to be measured in order to get a complete idea of the scaling of the wall pressure.

The results of some previous researchers also indicate that the wall pressure spectrum scales with mean wall shear stress, especially for frequencies corresponding to the smaller structures in the flow [2].

6. Beeler, G. B., (1986), "Turbulent Boundary-Layer Wall Pressure Fluctuations Downstream of Tandem LEBU", AIAA Journal, vol. 24, no. 4, pp. 689-691, (April 1986).

7. Cox, Albert W., *Sonar and Underwater Sound*, Lexington Books, Lexington, MA (1974), pg. 117.

1.2. Objectives

The objectives of this work were 1) to find the manipulating device which created the most rapid and largest decrease in local friction coefficient downstream of the device, 2) to measure and describe the changes in the boundary layer across and downstream of the device, 3) to make point measurements of mean wall shear and wall pressure spectra, 4) to verify that pressure spectra scale with wall shear in the non-equilibrium flow, 5) to make streamwise and spanwise cross-spectral measurements in the non-equilibrium flow for the sake of describing the convective behavior and structure of the flow.

2. EXPERIMENT DESCRIPTION

2.1. The Device

A honeycomb placed inside the boundary layer was chosen as the device best suited for the goal of rapid downstream local friction reduction. A survey of the local friction coefficient profiles under manipulated boundary layers reported by other researchers [8,9,10,11] was done as a means of selecting likely candidates for the manipulator desired for these experiments. Bushnell makes brief mention of a honeycomb placed inside the turbulent boundary layer offering as much as 50% reduction in wall shear.

Any device which alters the large scale structure of the boundary layer through the use of stream-wise elements in the outer portion of the boundary layer can be thought of as having two effects; "wake" effects and "plate" effects. The wake which the element sheds must have vorticity in both senses and that which is opposite to the sense of the boundary layer forms a barrier to the penetration of momentum from structures in outer portion of the boundary layer to the inner. The presence of an element in the boundary layer creates a new no-slip condition and thereby serves to suppress fluctuating velocities. The presence of these two conditions ought to create a relatively quiescent, "re-laminarized" region

8. Hefner, J. N., Weinstein, L. M., & Bushnell, D. M., (1980), "Large-Eddy Breakup Scheme for Turbulent Viscous Drag Reduction", *Progress in Astronautics and Aeronautics*, vol. 72, pp. 110-127.

9. Anders, J. B., Hefner, J. N., and Bushnell, D. M., (1984), "Performance of Large Eddy Breakup Devices at Post-Transitional Reynolds Numbers", AIAA Paper 84-0345, (Jan. 1984).

10. Corke, T. C., Guezennec, Y., and Nagib, H. M., (1979), "Modification in Drag of Turbulent Boundary Layers Resulting from Manipulation of Large-Scales Structures", Symposium on Viscous Drag Reduction, Dallas, Tex., Nov. 7-8.

11. Frei, D., and Thomann, H., (1980), "Direct Measurement of Skin Friction in a Turbulent boundary Layer with a Strong Adverse Pressure Gradient", *J. Fluid Mechanics*, vol. 101, part 1, pp. 79-95.

downstream of the device. A honeycomb may be less effective at shedding counter-vorticity and more effective at breaking up large structures than the LEBU because of the honeycomb's vertical elements.

A honeycomb essentially introduces three new length scales into the description of the manipulated boundary layer; the comb height, diameter, and streamwise length. Figures 1a and 1b are a sketch and a photograph of the device. In this experiment, all three were kept constant and the boundary layer thickness incident upon the manipulator was varied. A fourth variable introduced by the presence of the manipulator is the downstream distance from it to the point of measurement. The honeycomb dimensions were chosen based on the boundary layer thickness and the corresponding large eddy sizes. The "natural" boundary layer thickness on the walls of the duct was estimated through use of the code given by Cebeci [12]. The comb height was chosen to be no higher than the boundary layer thickness in order to not introduce any irrotationality into the essentially inviscid freestream. The hole size ($d \approx 400$) was chosen so that the largest eddies would be most affected (i.e. the comb height to hole size ratio would be less than ten). This is much larger than the Taylor microscale for the Reynolds numbers of the experiment. After Lumley [13],

$$\frac{\lambda}{\delta} \approx \sqrt{\frac{15}{Re_{\delta}}} \approx 0.02.$$

The boundary layer was calculated to be approximately one inch in thickness before entering the device. The comb used was made from aluminum, had a mean hole size of 1/4", and a web thickness of .004". The honeycomb's streamwise length varied with distance from the wall with the narrowest part being in the outer part of the layer and the widest part being at the wall. This was done to avoid creating enough blockage to separate the flow and create a quasi-recirculating region downstream of the device. The order of the pressure drop in the outermost parts of the comb can be estimated by,

$$\frac{\Delta p}{q} \approx \frac{\pi d_c l_c \mu \frac{\Delta U_c}{d_c}}{\frac{\pi}{4} d_c^2 q} = \frac{8 \nu l_c}{U d_c^2} \approx 0.0008.$$

This profile also serves to be screen-like (tending to decrease turbulent length scale) in the outer portions of the boundary layer where eddies are relatively large and velocity fluctuations relatively low and tube-

12. Cebeci, T. and Bradshaw, P., *Momentum Transfer in Boundary Layers*, Hemisphere Pub. Corp., Washington, (1977), p. 194.

13. Tennekes, H., and Lumley, J. L., *A First Course in Turbulence*, M.I.T. Press, Cambridge, Ma. (1981), pg. 67.

like (tending to suppress fluctuating velocities) in the inner portions of the layer where length scales are small and fluctuating velocities are large.

2.2. Wind Tunnel

All tests were carried out in the M.I.T. Acoustic and Vibration Laboratory low-turbulence, low-noise wind tunnel. It was constructed and described by Hanson [14] and is shown in Figure 2. The tunnel's blower motor has recently been replaced by a General Electric Model DC-300 speed controlled motor. Drift of the blower speed from the desired speed set point no longer occurs with the new motor. The experiments described here were run with the tunnel in the closed duct configuration. The duct is 15"x15" in cross-sectional area and approximately 13' in length. The maximum core flow velocity through the duct is approximately 50 meters per second.

Four tunnel nominal mean flow speeds were chosen for most of the tests; two the same as Farabee's [2] operating points (16 m/s and 28 m/s), one between the two (25 m/s), and the fourth at a higher speed (33 m/s). They shall hereafter be referred to as speeds 1, 2, 3, and 4, respectively.

The honeycomb manipulator was fastened with fine wire to the wall of the tunnel on the side which was upstream of the shear- and pressure-measuring insert which will be described later. The data are presented for various streamwise locations downstream of the honeycomb and this was accomplished by moving the honeycomb to different stations along the tunnel wall rather than moving the insert. The honeycomb was placed at three stations upstream of the insert which shall be referred to as stations 1, 2, and 3 and correspond to approximately 17.5, 50, and 80 pre-manipulator displacement thicknesses separation between honeycomb and measuring station.

All cracks between tunnel sections and at the instrumentation insert were puttied and sanded smooth with 600 grit sandpaper. The tunnel wall downstream of the comb was sanded as well.

14. Hanson, C. E., (1969), "The Design and Construction of a Low Noise, Low Turbulence Wind Tunnel", Acoustics and Vibration Lab M.I.T. Rept. no. 79611-1.

2.3. Pressure Measurements

All pressure measurements were made on the wall of the duct at Reynolds numbers based on distance from the end of the contraction ranging from 2.91×10^6 to 5.96×10^6 . Two wall inserts were used to mount the microphones. One insert held both a single microphone and the surface-fence wall-shear stress gage (which will be described later) flush with the wall at the same downstream location. It is shown with the surface fence in place in Figure 3. The second insert was the same insert used by Blake [1] to make convective velocity measurements. It is shown in the built-up test section in Figure 4. It consisted of a polished circular plug flush-mounted in a square plate. The plug had a line of 1/8" holes along its diameter. By placing a pair of microphones in selected pairs of holes, convective speeds and coherence of pressure waves in the turbulence could be measured. During all these measurements, all unused holes were filled with putty and made flush with the surface by shaving off with a razor any putty which protruded above the wall surface. The microphones were brought flush with the insert surface by sliding them through the back side of the insert until they protruded above the tunnel wall surface and then were pushed back to the wall using a short straight edge to stop the motion when the cap surface met the wall surface. All wall pressure measurements were made with Bruel & Kjaer Model 4138 1/8" microphones covered by pinhole caps having a hole diameter of 1/32".

The microphone signals were amplified by a pair of Bruel & Kjaer Model 2607 measuring amplifiers before being sent out of the wind tunnel blockhouse to the spectral analyzer. Before each run both microphone/follower/amplifier/analyzer channels were calibrated using a Bruel & Kjaer Model 4220 pistonphone which produced a 500 Hz tone at 124 db. Before most runs the microphones were baked for forty-five minutes at 200°F to drive off any moisture which might be present on the diaphragm surfaces and cause arcing.

2.4. Velocity Measurements

Profiles of the streamwise mean and fluctuating velocity fields with and without a manipulating device were recorded. A TSI Model 1261R U-type probe placed in the flow was balanced by a DANTEC Model 56C01/17 Constant Temperature Anemometer. The probe was mounted on a DISA Model

55A42 sting and inserted through the side of the tunnel opposite the wall pressure/wall shear measuring insert. The sting position was precisely set by mounting it in a screw traverse having a positioning resolution of .005 inch. It is shown in Figure 5. The anemometer was calibrated against a pitot-static probe placed in the core flow of the tunnel. The pitot-static probe transducer, a Validyne Model CD23, had in turn been calibrated against a Betz water manometer. Both the Validyne transducer and the anemometer were calibrated before each profile measurement. The anemometer response was linearized by first recording a raw volts versus dynamic head schedule with a data acquisition program on the HP-1000 computer and then fitting a fifth order polynomial to the curve. All test measurements were translated to velocity using this curve.

During the experiments, velocity sampling was done with the HP-1000 computer. Approximately 100,000 samples were taken at each y value in order to reduce the deviation of the average velocity from the true velocity to .01 meters per second.

2.5. Shear Measurements

The measurement of mean wall shear offers some keen experimental challenges. The primary challenges have to do with intrusion into the flow field and calibration.

A sublayer surface fence was chosen as the probe for wall shear measurement. It consists of a flush-mounting plug inside of which is a plate which separates two chambers and which protrudes a very short distance into the flow. Each chamber has a port to a pressure transducer and another port to the wall surface beside the fence. When a boundary layer is established moving perpendicular to the fence, the flow separates on the back of the fence and a pressure drop Δp develops across the fence. If the fence is short enough that it is in a region where viscous momentum terms dominate the convective terms, the response of the probe will be linear. The surface fence built for these experiments was approximately the height of the viscous sublayer and therefore interacted with the flow field in a way which made the convective terms significant. The calibration curve of the fence, Figure 14, shows the wall shear stress $\tau_w \propto \Delta p^{2/3}$, a weak non-linearity for all but the smallest values of τ_w . A sketch is shown in Figure 6. It has been described by Winter, Fernholz, and Head and Rechenberg [14,15,16,17]

and has several additional advantages over other measurement techniques; those being high sensitivity and directionality.

The benefit of remaining inside the viscous sublayer is that the measurement no longer depends on a knowledge of the shape of the overlap layer but rather, as Coles [18] has pointed out, on a constant stress layer which must exist very near the wall for any type of boundary layer. This is unlike the oft-used Preston tube which is commonly calibrated in flows in which the top surface of the tube is as high as several hundred y^+ [19]. Such a calibration then requires a knowledge of the behavior of the "law of the wall" and how it might be modified by boundary layer manipulation.

2.6. Spectral Measurements

Point spectra were measured with the support of the HP-1000 computer and the program P_SPECT4 which contains the Fast Fourier Transform (FFT) subroutine given by Newland [20]. The subroutine calculates

$$P_m = \frac{1}{N} \sum_{l=0}^{N-1} p_l e^{-i(2\pi pl/N)}$$

One hundred spectra each having 2048 points were taken and averaged at each flow condition. Data were sampled at 50 kHz and the resulting bandwidth was 12.2 Hz.

Cross spectra were measured using the GenRad Model 2515 16 channel analyzer. All had a 2 Hz bandwidth and 1000 spectra made up each average. The continuous cross-spectrum is expressed as

$$\Phi(\vec{P}, \omega) = \frac{1}{2\pi} \int_{-\infty}^{\infty} R_{12}(\vec{P}, \tau) e^{i\omega\tau} d\tau$$

The analyzer does its analysis by performing a direct Fourier transform on each channel and then

14. Winter, K. G., (1977), "An Outline of the Techniques Available for the Measurement of Skin Friction in Turbulent Boundary Layers", *Prog. Aerospace Sci.*, vol. 18, pp. 1-57.
15. Dengel, P., Fernholz, H. H., and Hess, M., (1986), "Skin-Friction Measurements in Two- and Three-Dimensionally Highly Turbulent Flows With Separation", *First European Turbulence Conference, Lyon, France, (July 1986)*.
16. Vagt, J. D., and Fernholz, H., (1973), "Use of Surface Fences to Measure Wall Shear Stress in Three-dimensional Boundary Layers", *Aeronautical Quarterly*, vol. 24, part 2, pp. 87-91, (May 1973).
17. Head, M. R., and Rechenberg, I., (1962), "The Preston Tube as a means of Measuring Skin Friction", *J. Fluid Mechanics*, vol. 14, pp. 1-17.
18. Coles, D. E., "The Law Of The Wall In Turbulent Shear Flow", *50 Jahre Grenzschichtforschung*, (H. Gortler & W. Tollmien, eds.), F. Vieweg und Sohn, Braunschweig, pp. 153-163.
19. Goldstein, R. J., ed., *Fluid Mechanics Measurements*, Hemisphere, New York, (1983), pp. 559-611.

computing the auto-power spectra which is the DFT multiplied by its complex conjugate. It also retains the single channel DFTs and takes complex conjugate products to get the phase and power of the cross-spectra. The total bandwidth for each cross spectra was approximately twice the frequency at which the coherence of the signal fell below .0025. Both signals were sent through anti-aliasing filters set to low pass frequencies below the sampling rate. All spectra were taken at 29 m/s.

3. EXPERIMENTAL RESULTS

3.1. Mean Velocity

The first set of velocity measurements were of the clean (i.e. unmanipulated) tunnel wall boundary layer. These profiles were validated in much the same way Blake [1] did in his smooth wall measurements. The dimensional profile was plotted in velocity versus $\log y$ coordinates and a line was fitted by regression analysis to the points which appeared to represent the "law of the wall" layer. It has been mentioned before that the distance of the probe from the wall could be measured with a sufficiently great precision. It was not, however, sufficiently "zeroed" until this point in the reduction. Any misjudgement in the zero value of y would show up as a curvature of the log layer on the semi-log plot. The profile was properly "zeroed" by iteratively adjusting the y origin until the most colinear set of points resulted on the plot. It was found that the zero value on the traverse changed for different tunnel speeds and the change was of such magnitude and direction as to make it appear the wooden walls of the duct were bending slightly and progressively inward with increasing tunnel speed.

Figure 7 displays the boundary layer mean profiles nondimensionalized by outer-layer variables and is a demonstration of the similarity of the clean wall profiles for different tunnel Reynolds numbers. Figure 8 shows the same profiles in "law of the wall" coordinates plotted against Coles [18] tabulated values for the "standard" mean profile. The logarithmic layer is described by the equation

20. Newland, D. E., *An Introduction to Random Vibrations and Spectral Analysis*, Longman, Inc., New York, (1983), pg. 220.

$$\frac{\bar{u}}{u^*} = C_1 \log\left(\frac{yu^*}{\nu}\right) + C_2$$

The value of friction velocity for each profile was determined by reguessing the "log layer" points until the value of C_2 resulting from the regression made the line through them coincide with the line of Coles.

Figure 9 is a set of profiles of the manipulated boundary layer again normalized by outer-layer variables. In all cases, the shape factor has increased; typically by approximately 0.08 with no clear trend with downstream distance being apparent. These plots are now not necessarily to be called self-similar because new length scales have been introduced to the outer variables; those being primarily the height of the honeycomb and the comb diameter. Figure 10 shows the same profiles scaled by comb height. What is apparent from the plots are the global changes in the profile shapes compared to the unmanipulated ones. What is apparent from the data, particularly at station 1, is the "stepping" of the profile left by the internal "boundary layer" growth in the individual combs. The profiles at station 2 have an inflection point at approximately one comb height. Near the wall, the value of $\frac{d\bar{u}}{dy}$ is comparatively low while farther from the wall, near the outer portion of the boundary layer, it is comparatively high. If one thinks of this profile as an indicator of mean vorticity in the boundary layer, the manipulated profile has shifted the vorticity distribution outward from the wall and thereby lessened the transport of high momentum fluid to the inner portions of the layer.

Figure 11 is a set of "law of the wall" plots of the manipulated boundary layer at various downstream locations plotted along with the Coles data. All look very much like an equilibrium profile which has been misscaled by using a friction velocity value which is too low. All of the data are shifted in the direction of larger u^+ for the same y^+ with only the profiles at the location furthest downstream showing an indication of strong similarity based on inner variables. The profiles taken at station 2 have similar shape but their separation from each other on the plot in such a regular fashion would suggest they may scale with Reynolds numbers based on comb-related variables such as manipulated displacement thickness, distance downstream, or comb height.

The skin-friction coefficients corresponding to these friction velocity values are plotted against

Re_{δ^*} and $\Delta x/\delta^*$ in Figures 12 and 13 along with an empirical relation given by White [21]. It is

$$C_f \approx 0.0128 Re_{\delta^*}^{-1/4}$$

White estimates the curve to be accurate to within four percent and the data are at most three percent from the line. The skin friction coefficients of the manipulated flow are from 24% to as much as 38% of the clean flow values and appear to have the trend of increasing with increasing Re_{δ^*} . Friction coefficients appear, for the region measured at least, to be decreasing with increasing downstream distance. It would be expected, however, that an equilibrium boundary layer would reestablish itself by some distance downstream and that the friction coefficient would return to the expected values.

The calibration curve for the surface fence is shown in Figure 14. It shows the expected and desired linear relationship between wall shear and signal. Again, the values of wall shear were gotten by fitting of the respective logarithmic portions of the profiles.

3.2. Turbulence Levels

Figures 15 and 16 are plots of turbulence level normalized by friction velocity versus distance from the wall normalized by displacement thickness. Figure 17 is of the same manipulated profiles but nondimensionalized by comb height. The manipulated profiles have comparatively higher intensities farther from the wall and lower levels near the wall. An example of the "plate" effects described earlier is that just downstream of the comb and within one comb height of the wall, the manipulated profiles have a certain amount of "stagger" to them because of the individual wakes left by the elements of the comb. The profiles taken at station 2 have the expected increase coinciding with the inflection point in the profiles.

3.3. Wall Pressure

3.3.1. Point Spectra

Figure 18 is a plot of total r.m.s. pressure at certain points downstream of the honeycomb at two tunnel speeds. The dotted and dashed lines represent r.m.s. pressures found in the equilibrium flow. The

21. White, F. W., *Viscous Fluid Flow*, McGraw-Hill, New York, (1974), pg. 495.

data were gotten from the values of the respective autocorrelation functions at zero time delay. Because the 4138 Microphone is not intended to measure frequencies below 10 Hz and because, as Blake [1] has reported, large amplitude tunnel disturbances exist below 70 Hz, the signals were high-passed at 70 Hz before being analyzed. The maximum reduction in wall pressure is not immediate but rather approximately fifty displacement thicknesses downstream. In air, the reduction corresponds to as much as 4 db. Perhaps there is a zone immediately following the comb in which the wakes shed by the elements of the comb dominate the turbulence followed by a zone in which the free stream velocity and pressure gradient begin to reestablish an equilibrium flow.

Pressure spectral densities for the highest three tunnels speeds are shown in Figures 19-22. The spectra were smoothed by averaging each point in the spectra with its nearest ten neighboring points. Every tenth point is plotted. The points for which Corcos [22] has predicted a 3 db reduction in transducer response are marked with a caret on each figure. Nondimensionalization is done in the first three plots with free stream velocity, mean wall shear, and displacement thickness and in the second with transducer diameter instead of displacement thickness. The use of transducer diameter has been suggested by Foxwell [23] because much of the data he has collected for $\omega\delta^*/U_\infty > 1.3$ scale better on it than on displacement thickness. With the exception of station 1, the wall-shear & displacement thickness nondimensionalization makes the spectra fall very nearly one atop the other. Nondimensionalization by transducer diameter, if anything, is less capable of scaling high frequency data.

3.3.2. Streamwise Coherence

Figures 23-27 are plots of streamwise coherence against the phase of the cross spectrum along with an exponential envelope suggested by Farabee for equilibrium flow. Here coherence is defined as

$$\Gamma(r_1, r_3, \omega) = \sqrt{\frac{\Phi^*(r_1, r_3, \omega) \Phi(r_1, r_3, \omega)}{\Phi_1(\omega) \Phi_2(\omega)}}$$

It serves as a measure of the flow's ability to maintain its structure as it convects downstream. When

22. Corcos, G. M., (1963), "Resolution of Pressure in Turbulence", J. Acoustical Society of America, vol. 35, no. 2, pp. 192-199.

23. Foxwell, J. H., (1966), "The Wall Pressure Spectrum Under a Turbulent Boundary Layer", A.U.W.E. Tech. Note 218/66, (Aug. 1966).

plotted against phase for a given separation, each point nominally represents the phase change of an eddy of a given frequency as it convects from one microphone to the second and the degree to which it has lost its structure. Phase is given by

$$\alpha(\omega_0, r_1) = \tan^{-1} \frac{\Phi_i(\omega_0, r_1)}{\Phi_r(\omega_0, r_1)}$$

In all cases, there is a more rapid decay than the unmanipulated flow with coherence tending to move toward equilibrium with increasing downstream distance. It is possible, once again, that the measurements taken at station 1 are in the zone of structures which are of the order of the comb diameter and which typically have less distance to travel before decaying.

3.3.3. Spanwise Coherence

Figures 28-30 are similar plots of spanwise coherence against phase. Here no convective velocity can be discernable from the measurements and U_{cp} from the streamwise cross-spectrum for the same microphone separation at the same manipulator position is used along with ω and r_1 to calculate a phase relevant to the convecting structure. The notable feature of these plots is that the presence of the manipulator increases spanwise coherence and it is not clear why this is true. The comb may be shedding spanwise vortices off its top over a broad frequency range.

3.4. Convective Velocities

Figures 31-35 show pressure wave convective speed as a function of Strouhal number along with the line reported by Bull [24]. Phase convective speed was gotten from the phase component of the cross-spectrum and the relation

$$U_{cp} = \frac{\omega r_1}{\alpha(\omega, r_1)}$$

The data shows little difference from the equilibrium flow until $\omega \delta^* / U_\infty$ reaches 0.3, the number at which it has been supposed structures become small enough to convect in the boundary layer. The plot of U_{cp} for the largest microphone separation is treated as an anomolous case and may be the result of

24. Bull, M. K., Wilby, J. F., and Blackman, D. R., (1963), "Wall Pressure Fluctuations in Boundary Layer Flow and Response of Simple Structures to Random Pressure Fields", A.A.S.U. Report No. 243, (July 1963).

the microphones being placed in two zones of the flow which have fundamental differences. That the presence of the manipulator leaves the low frequency components unchanged may tell something about their source location. The manipulator dimensions are on the order of the boundary layer thickness; it is an outer layer device and it would be expected to alter most or all of the outer layer structure. The low frequency sources, then, may be in the inner layers and associated with events there, such as bursting.

4. CONCLUSIONS

1. The mean wall pressure spectral level of the manipulated flow scales better with mean wall shear stress than does the spectra of the unmanipulated flow.
 2. The manipulator decreases the streamwise and increases the spanwise coherence above $\omega\delta^*/U_\infty \approx 0.3$.
 3. The manipulator moves the active region farther from the wall.
 4. The manipulator reduces convective phase velocities for frequencies above $\omega\delta^*/U_\infty = 0.3$.
 5. The manipulator reduces mean wall shear stress and root-mean-squared pressure for downstream distances of the order of 100 displacement thicknesses.
 6. There is a zone immediately downstream of the manipulator in which the dominant manipulator length scale is the comb diameter and a second zone further downstream which is dominated by the comb height.
-

5. REFERENCES

- Anders, J. B., Hefner, J. N., and Bushnell, D. M., (1984), "Performance of Large Eddy Breakup Devices at Post-Transitional Reynolds Numbers", AIAA Paper 84-0345, (Jan. 1984).
- Beeler, G. B., (1986), "Turbulent Boundary-Layer Wall Pressure Fluctuations Downstream of Tandem LEBU", AIAA Journal, vol. 24, no. 4, pp. 689-691, (April 1986).
- Blake, W. K., (1970), "Turbulent boundary-layer wall-pressure fluctuations on smooth and rough walls", J. Fluid Mechanics, vol. 44, part 4, pp. 637-660.
- Brooks, T.F. and Hodgson, T.H., (1981), "Trailing Edge Noise Prediction From Measures Surface Pressures", J. Sound and Vibration, vol. 78, No. 1, pp. 69-117.
- Brown, Eugene F., (1987), "European Mtg. on Turbulent Drag Reduction", ESN 41-2, pg. 89.

Bull, M. K., Wilby, J. F., and Blackman, D. R., (1963), "Wall Pressure Fluctuations in Boundary Layer Flow and Response of Simple Structures to Random Pressure Fields", A.A.S.U. Report No. 243, (July 1963).

Cebeci, T. and Bradshaw, P., **Momentum Transfer in Boundary Layers** , Hemisphere Pub. Corp., Washington, (1977).

Coles, D. E., "The Law Of The Wall In Turbulent Shear Flow", **50 Jahre Grenzschichtforschung** , (H. Gortler & W. Tollmien, eds.), F. Vieweg und Sohn, Braunschweig, pp. 153-163.

Corcos, G. M., (1963), "Resolution of Pressure in Turbulence", J. Acoustical Society of America, vol. 35, no. 2, pp. 192-199.

Corke, T. C., Guezennec, Y., and Nagib, H. M., (1979), "Modification in Drag of Turbulent Boundary Layers Resulting from Manipulation of Large-Scales Structures", Symposium on Viscous Drag Reduction, Dallas, Tex., Nov. 7-8.

Cox, Albert W., **Sonar and Underwater Sound** , Lexington Books, Lexington, MA (1974).

Dengel, P., Fernholz, H. H., and Hess, M., (1986), "Skin-Friction Measurements in Two- and Three-Dimensionally Highly Turbulent Flows With Separation", First European Turbulence Conference, Lyon, France, (July 1986).

Farabee, Theodore M., (1986), "An Experimental Investigation of Wall Pressure Fluctuations Beneath Non-Equilibrium Flows", D. W. Taylor Naval Ship R & D Center, Rept. No. DTNSRDC-86/047, (May 1986).

Foxwell, J. H., (1966), "The Wall Pressure Spectrum Under a Turbulent Boundary Layer", A.U.W.E. Tech. Note 218/66, (Aug. 1966).

Frei, D., and Thomann, H., (1980), "Direct Measurement of Skin Friction in a Turbulent boundary Layer with a Strong Adverse Pressure Gradient", J. Fluid Mechanics, vol. 101, part 1, pp. 79-95.

Goldstein, R. J., ed., **Fluid Mechanics Measurements** , Hemisphere, New York, (1983), pp. 559-611.

Hanson, C. E., (1969), "The Design and Construction of a Low Noise, Low Turbulence Wind Tunnel", Acoustics and Vibration Lab M.I.T. Rept. no. 79611-1.

Head, M. R., and Rechenberg, I., (1962), "The Preston Tube as a means of Measuring Skin Friction", J. Fluid Mechanics, vol. 14, pp. 1-17.

Hefner, J. N., Weinstein, L. M., & Bushnell, D. M., (1980), "Large-Eddy Breakup Scheme for Turbulent Viscous Drag Reduction", **Progress in Astronautics and Aeronautics** , vol. 72, pp. 110-127.

Narayan, N. and Plunkett, R., (1985), "Pressure Cross Spectra in turbulent Boundary Layers in Water", ASME Winter Annual Mtg., Miami Beach, Fla., Nov. 17-22, NCA-Vol. 1, pp. 97-103.

Newland, D. E., **An Introduction to Random Vibrations and Spectral Analysis** , Longman, Inc., New York, (1983).

Tennekes, H., and Lumley, J. M., **A First Course in Turbulence** , M.I.T. Press, Cambridge, MA, (1972).

Vagt, J. D., and Fernholz, H., (1973), "Use of Surface Fences to Measure Wall Shear Stress in Three-dimensional Boundary Layers", *Aeronautical Quarterly*, vol. 24, part 2, pp. 87-91, (May 1973).

White, F. W., **Viscous Fluid Flow**, McGraw-Hill, New York, (1974).

Winter, K. G., (1977), "An Outline of the Techniques Available for the Measurement of Skin Friction in Turbulent Boundary Layers", *Prog. Aerospace Sci.*, vol. 18, pp. 1-57.

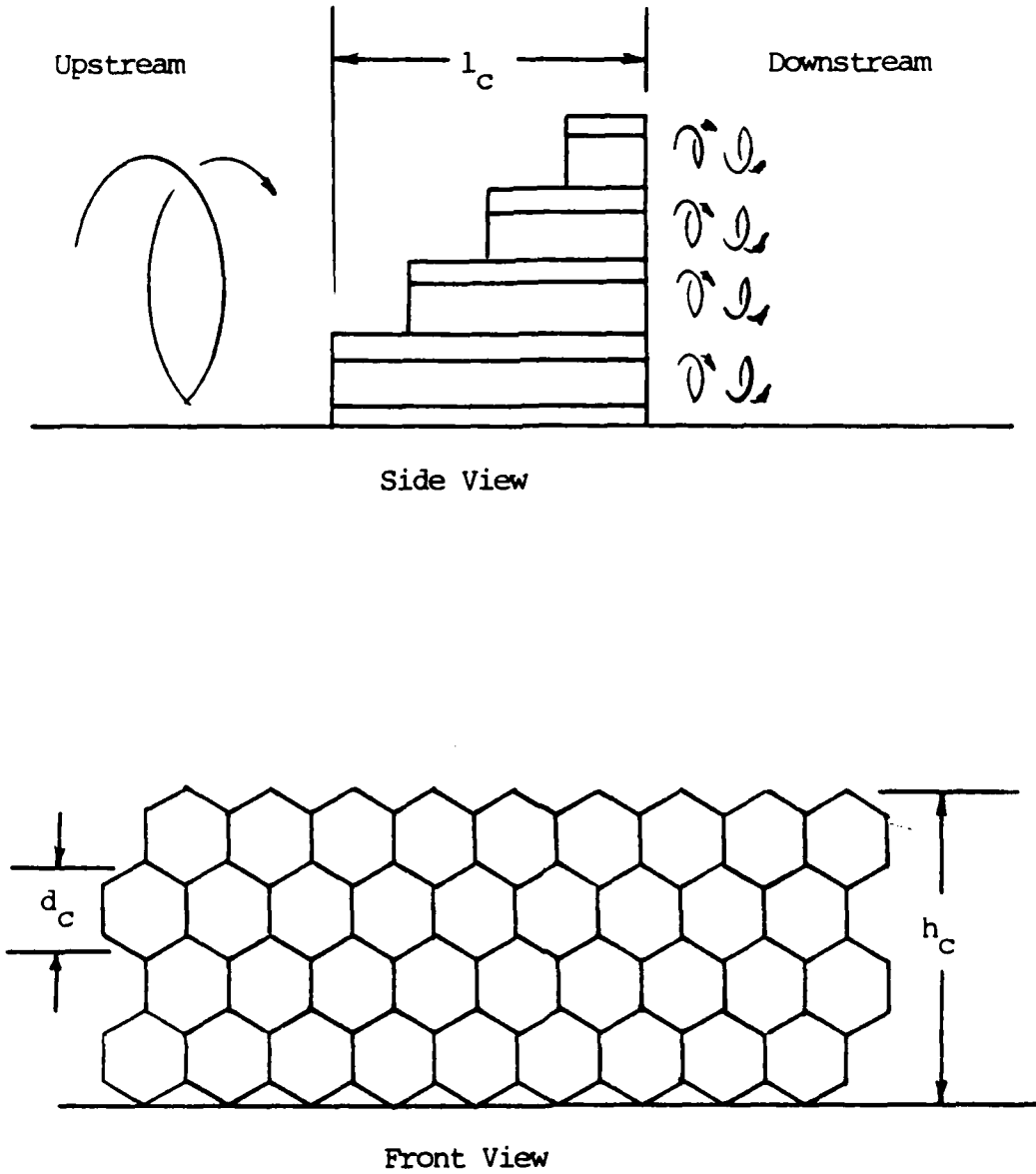


Figure 1a. Honeycomb Manipulator Sketch.

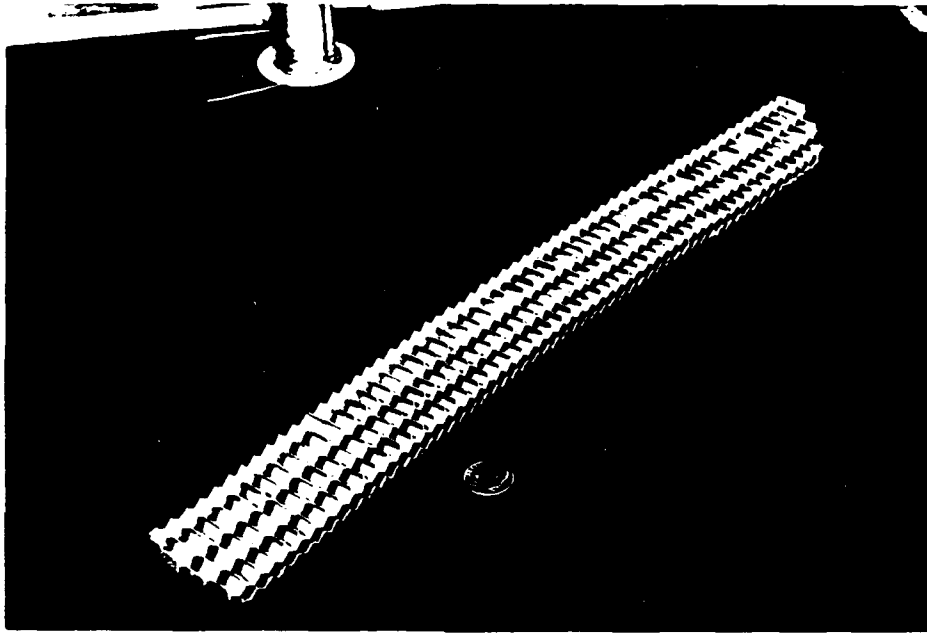
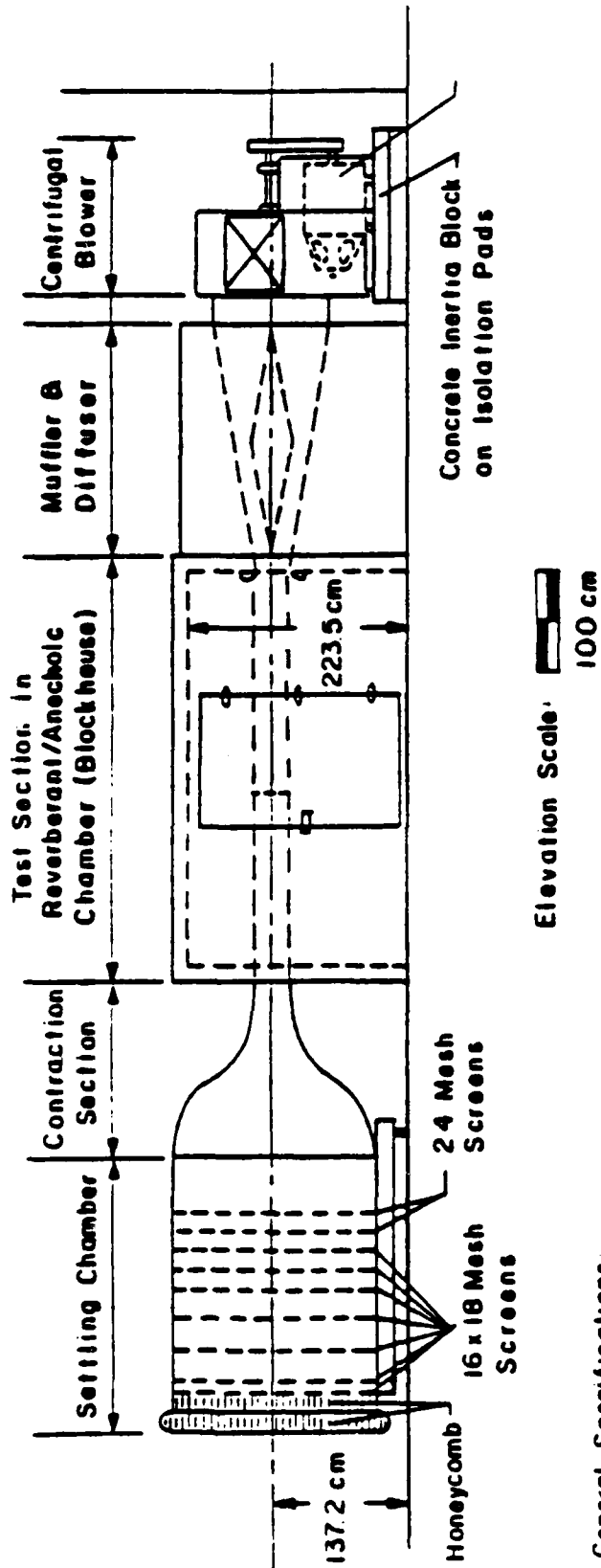


Figure 1b. Honeycomb Manipulator Photo.



General Specifications:
Contraction Ratio: 20:1
Test Section: 38cm x 38cm, shown in open duct configuration

WIND TUNNEL FACILITY -- ROOM 5-024
ACOUSTICS & VIBRATIONS LABORATORY
MASSACHUSETTS INSTITUTE OF TECHNOLOGY

Figure 2. Wind Tunnel Facility.

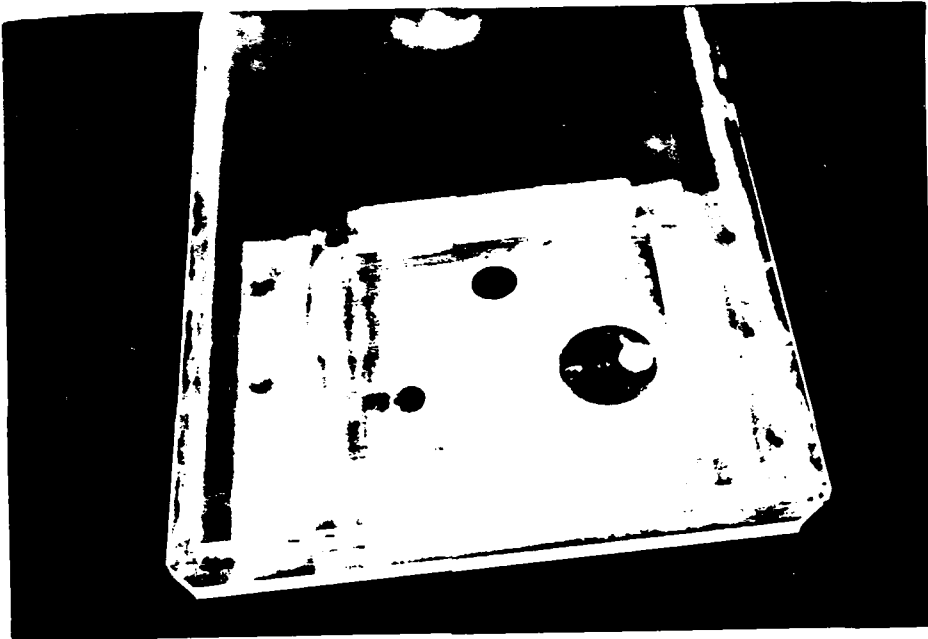


Figure 3. Point Spectra & Shear Measuring Insert.

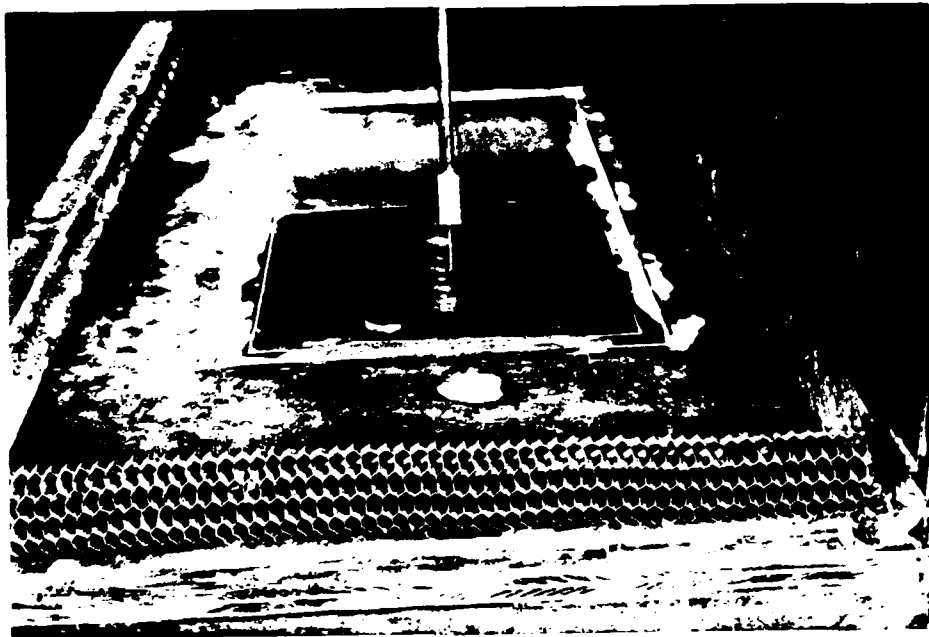


Figure 4. Cross-Spectral Insert and Test Section.



Figure 5. Hot Wire Traverse.

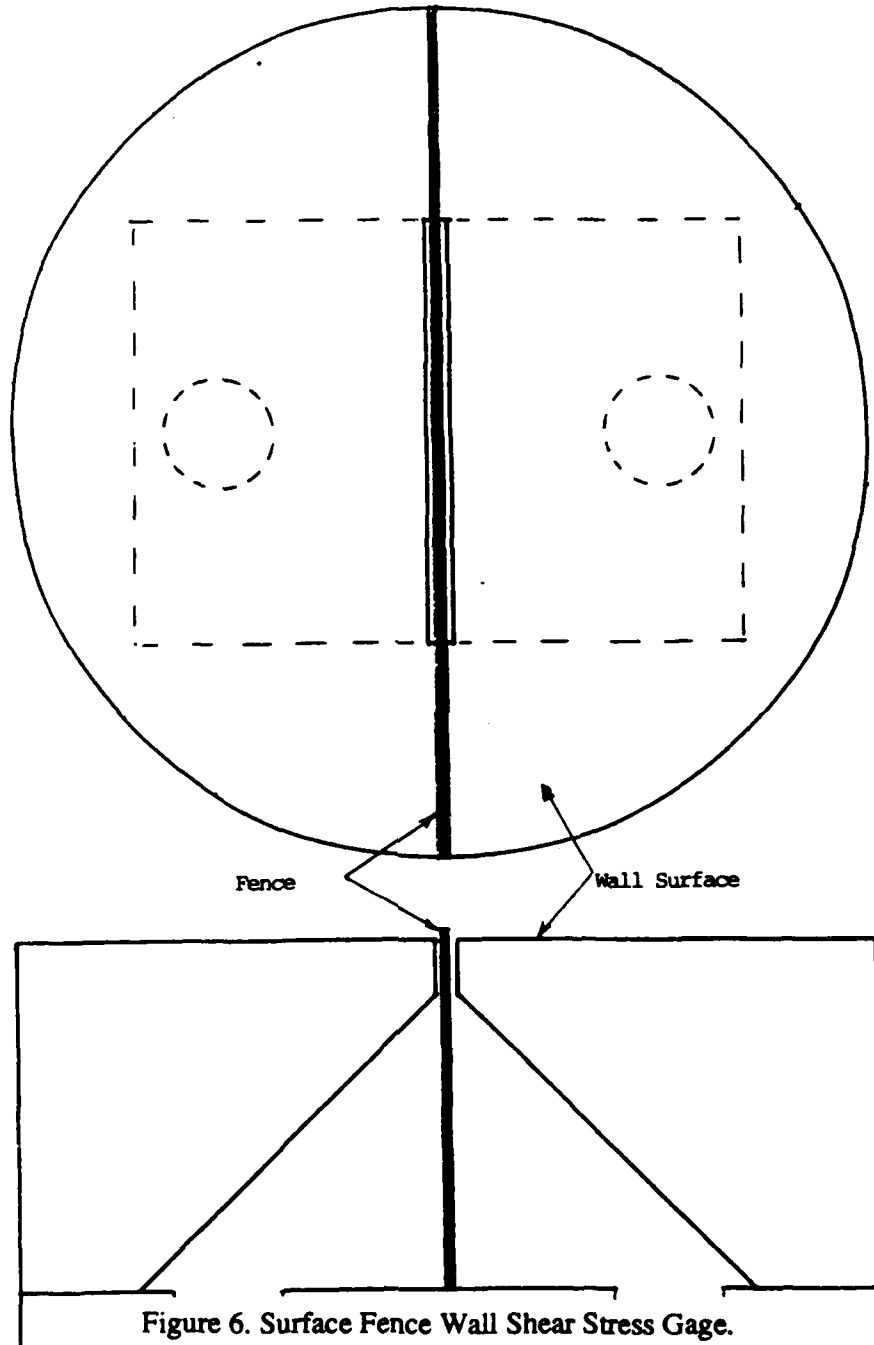


Figure 6. Surface Fence Wall Shear Stress Gage.

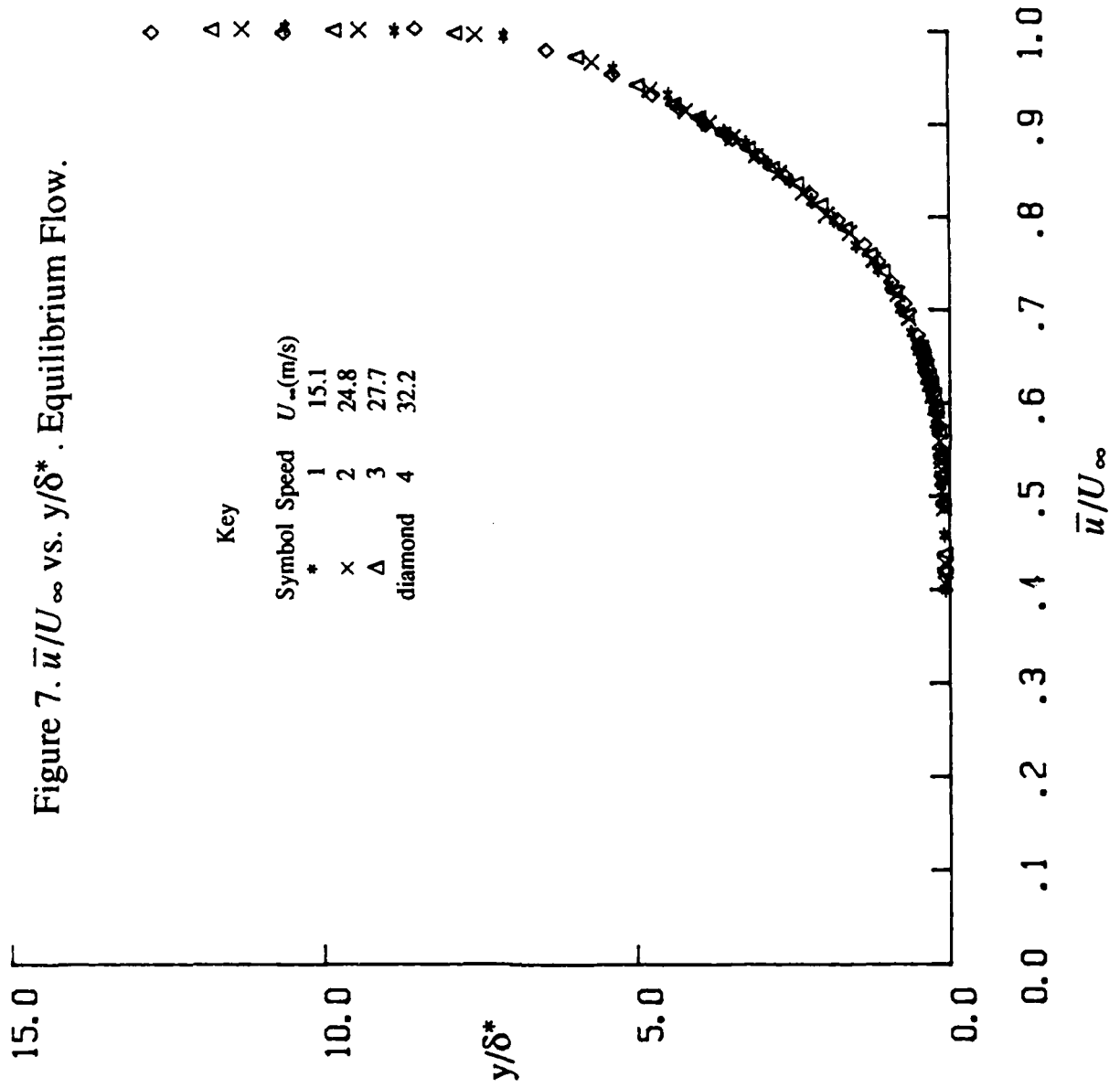
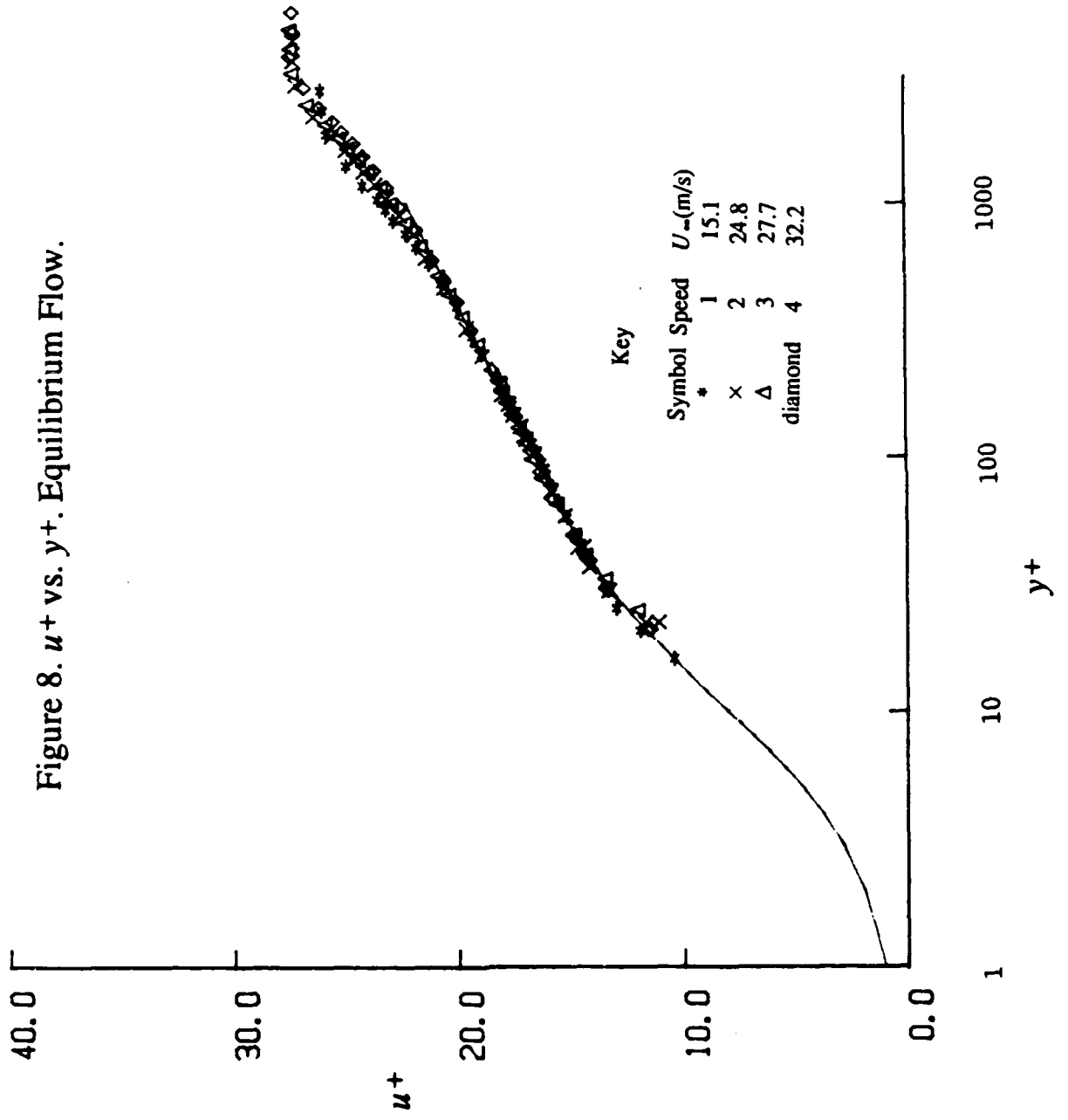
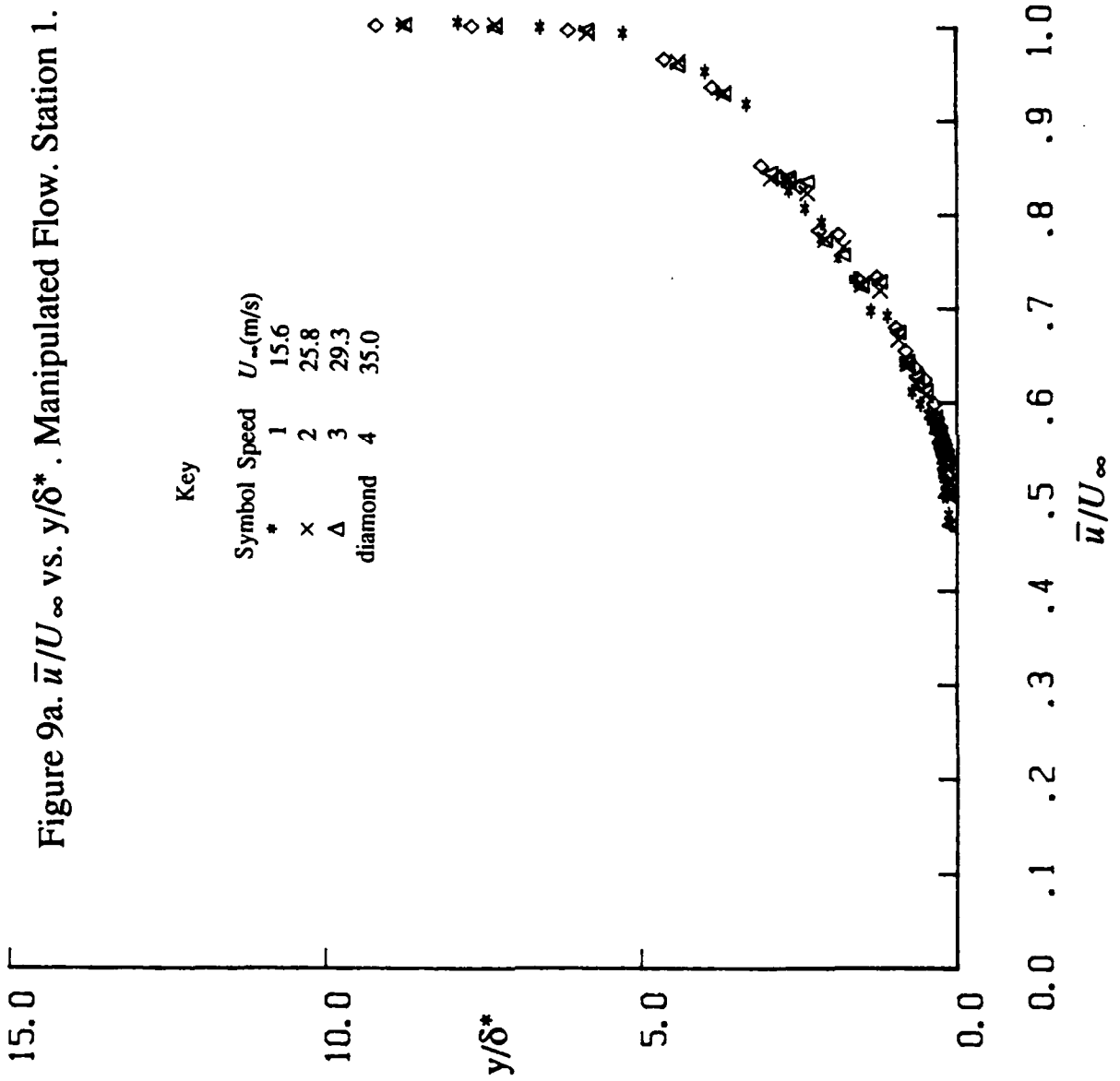
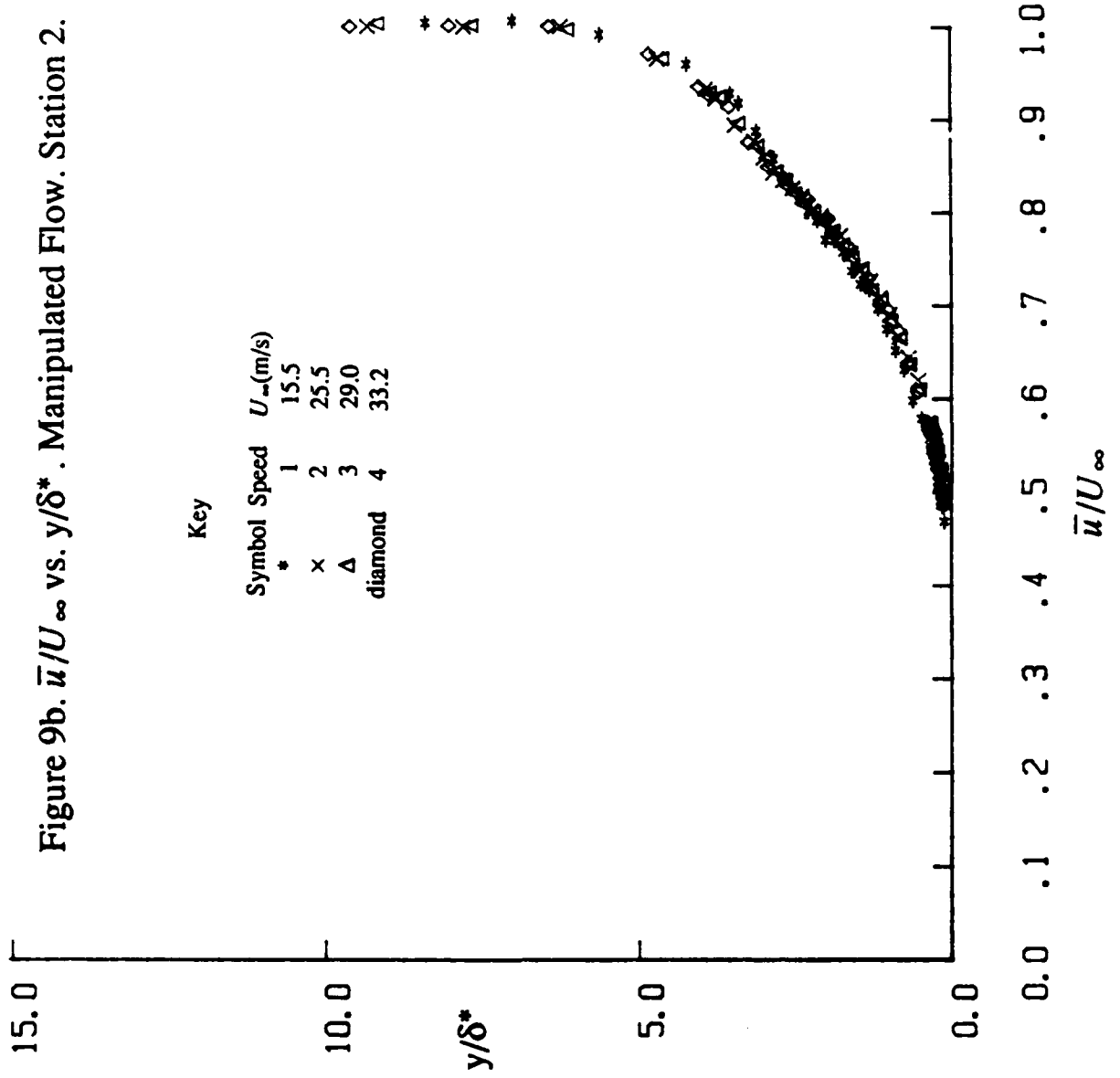


Figure 8. u^+ vs. y^+ . Equilibrium Flow.







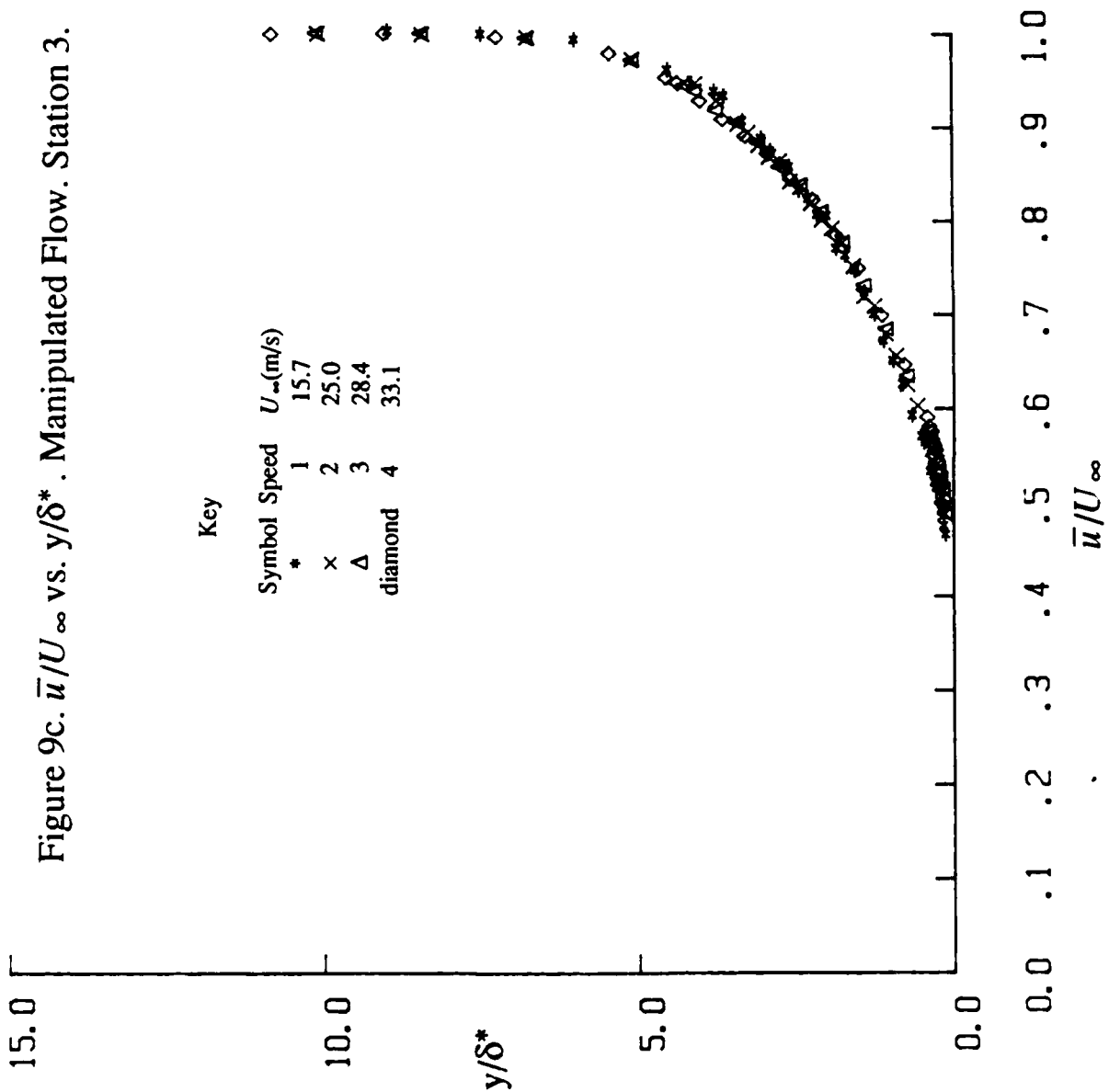


Figure 10a. \bar{u}/U_∞ vs. y/h_c . Manipulated Flow. Station 1.

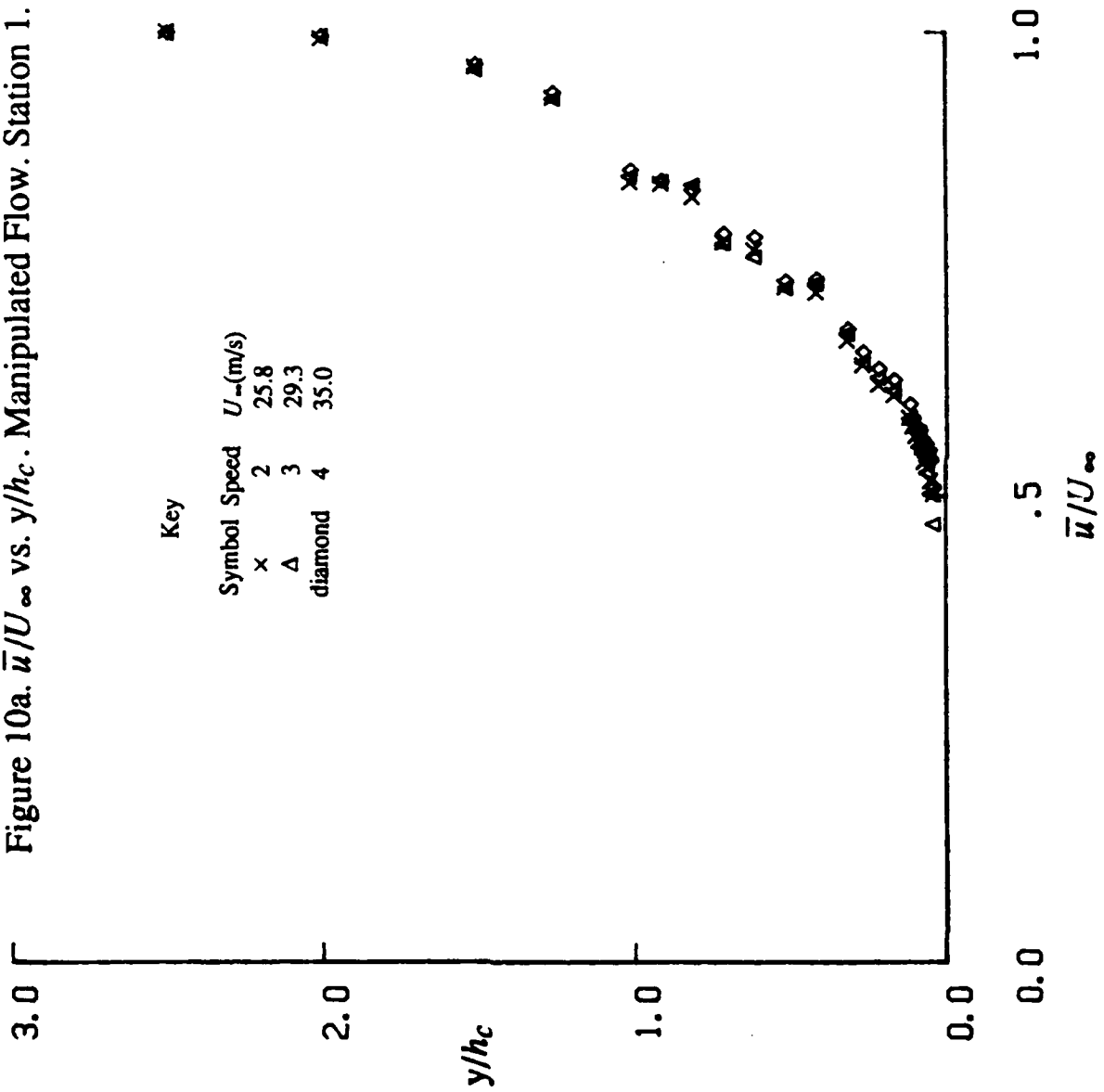


Figure 10b. \bar{u}/U_∞ vs. y/h_c . Manipulated Flow. Station 2.

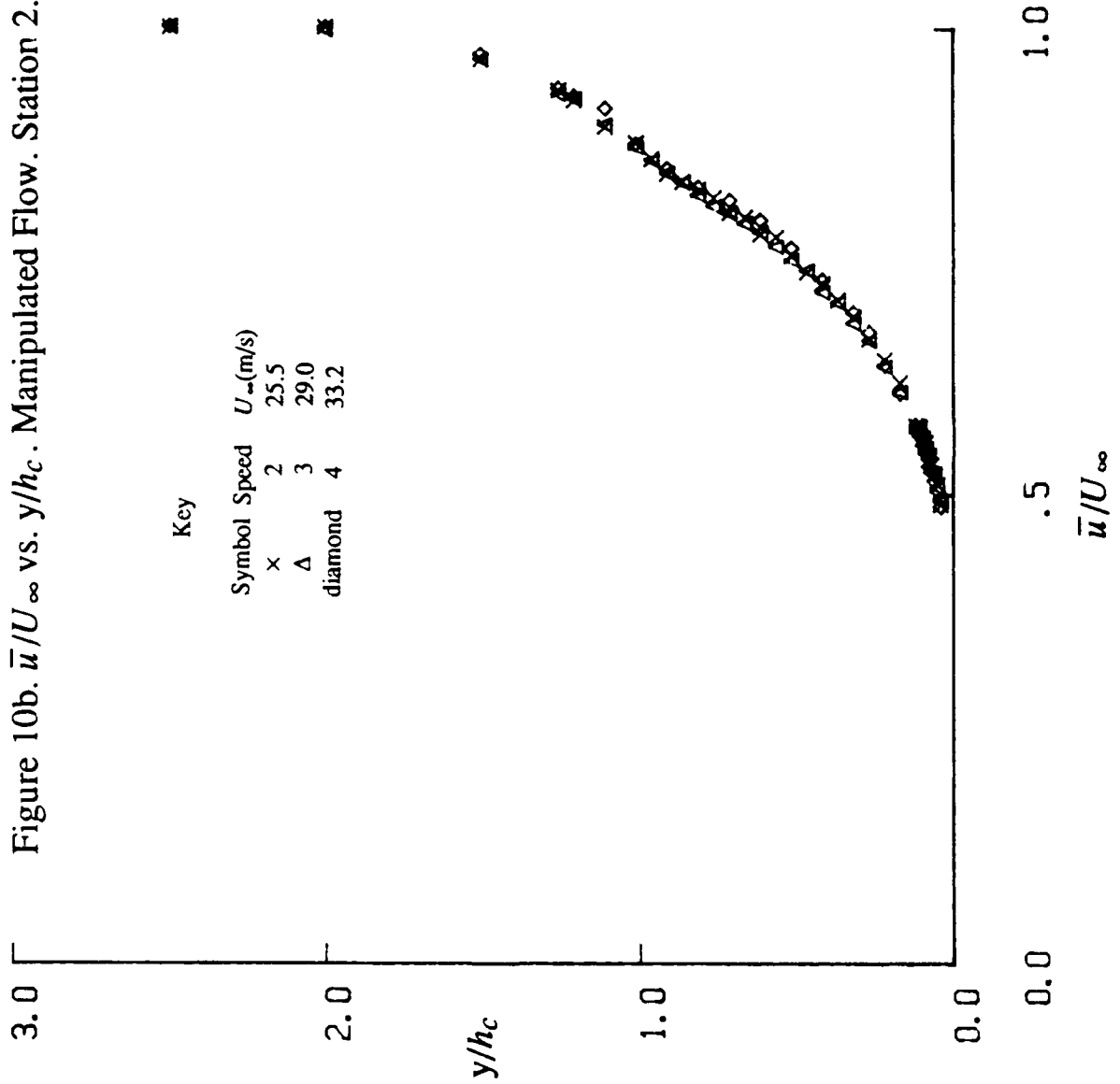
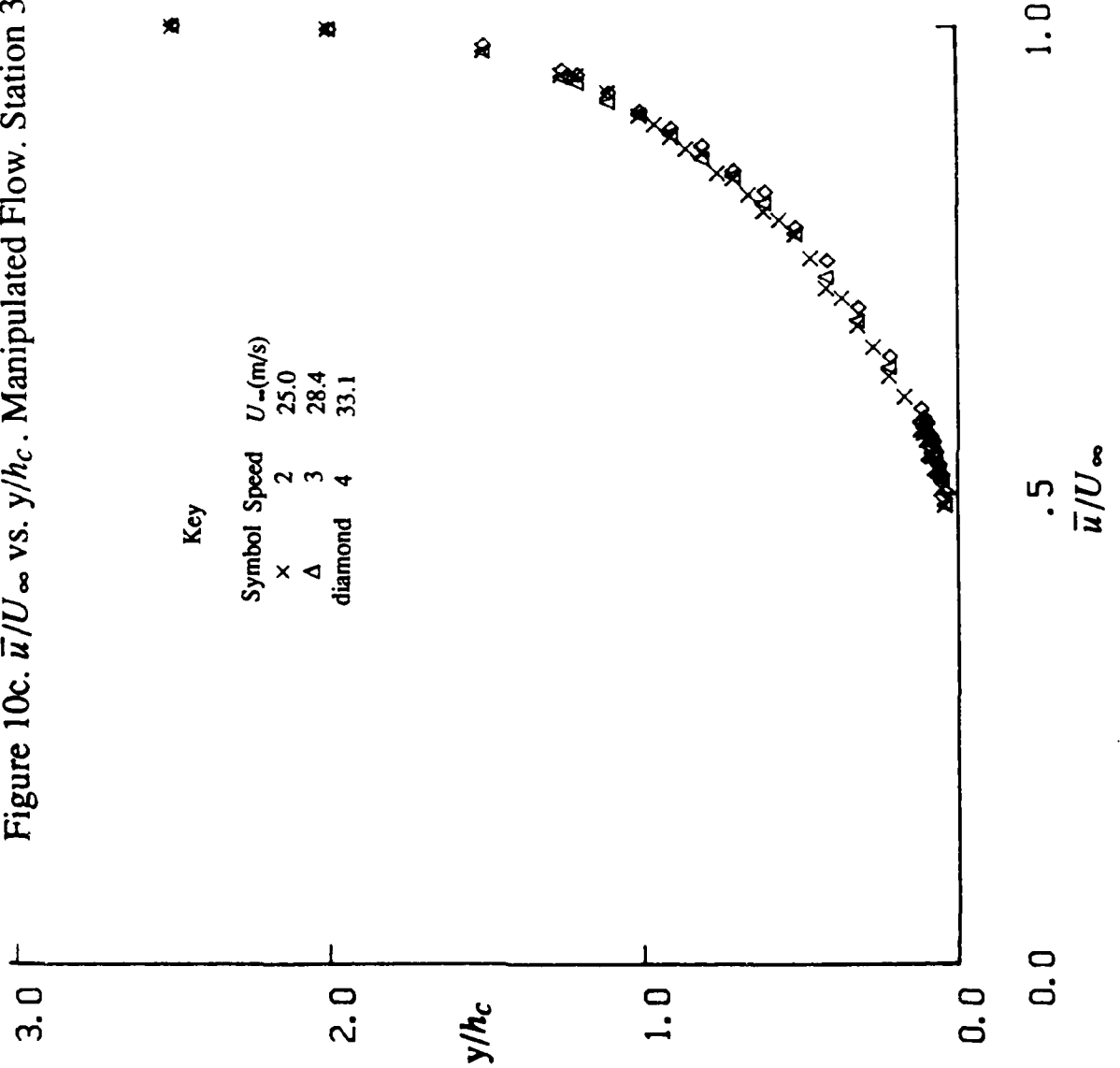


Figure 10c. \bar{u}/U_∞ vs. y/h_c . Manipulated Flow. Station 3.



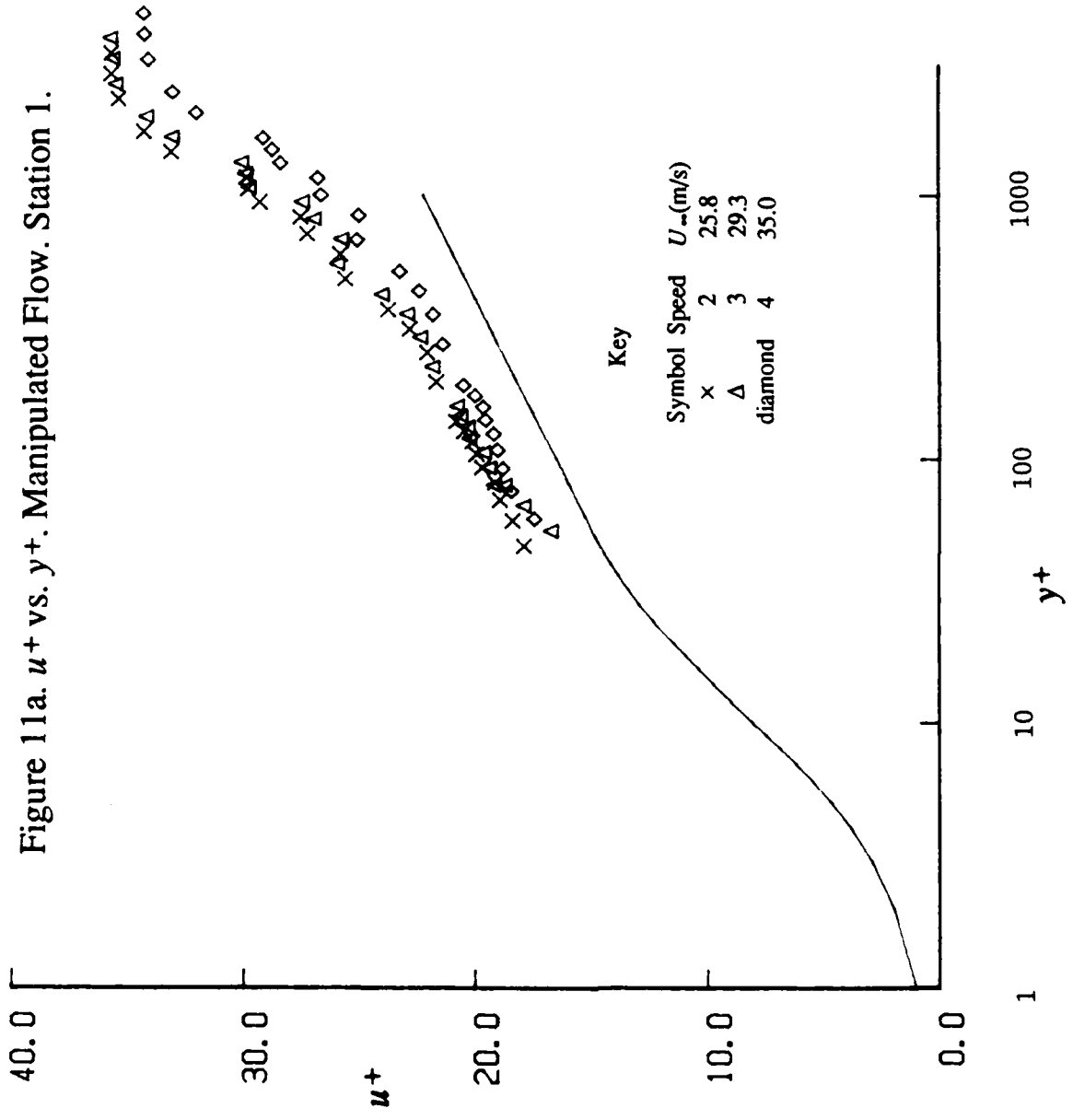


Figure 11b. u^+ vs. y^+ . Manipulated Flow. Station 2.

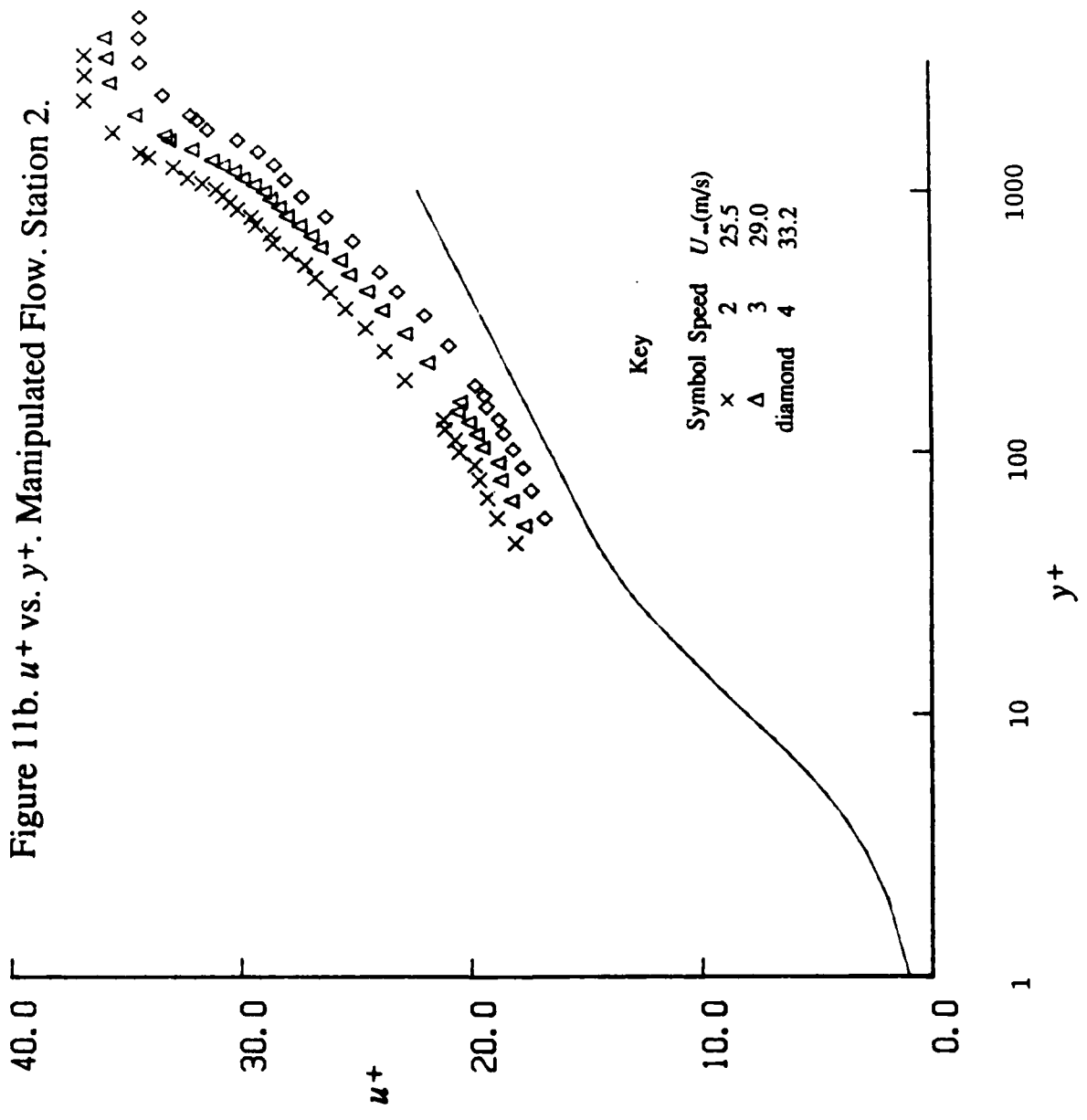
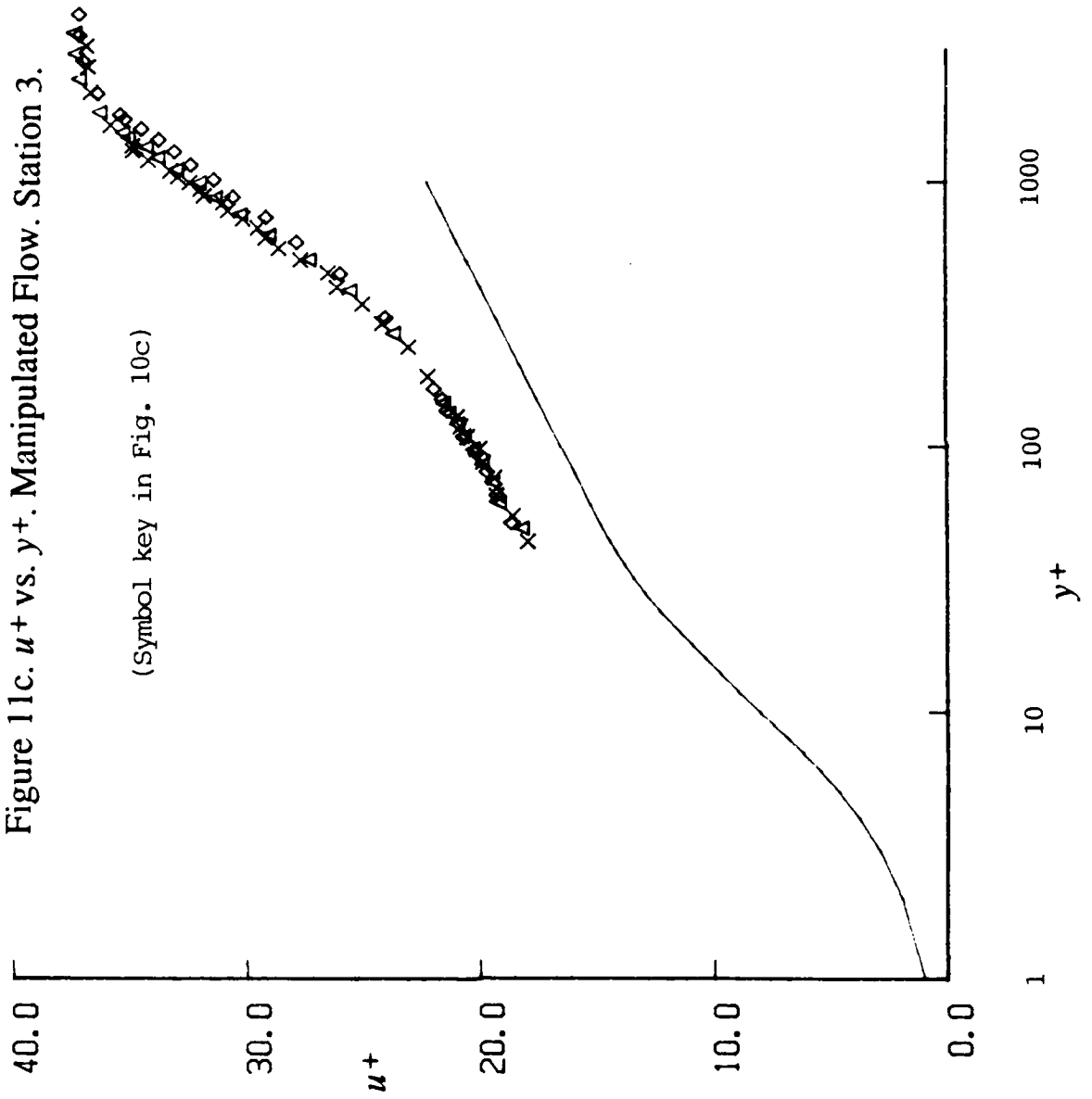


Figure 11c. u^+ vs. y^+ . Manipulated Flow. Station 3.



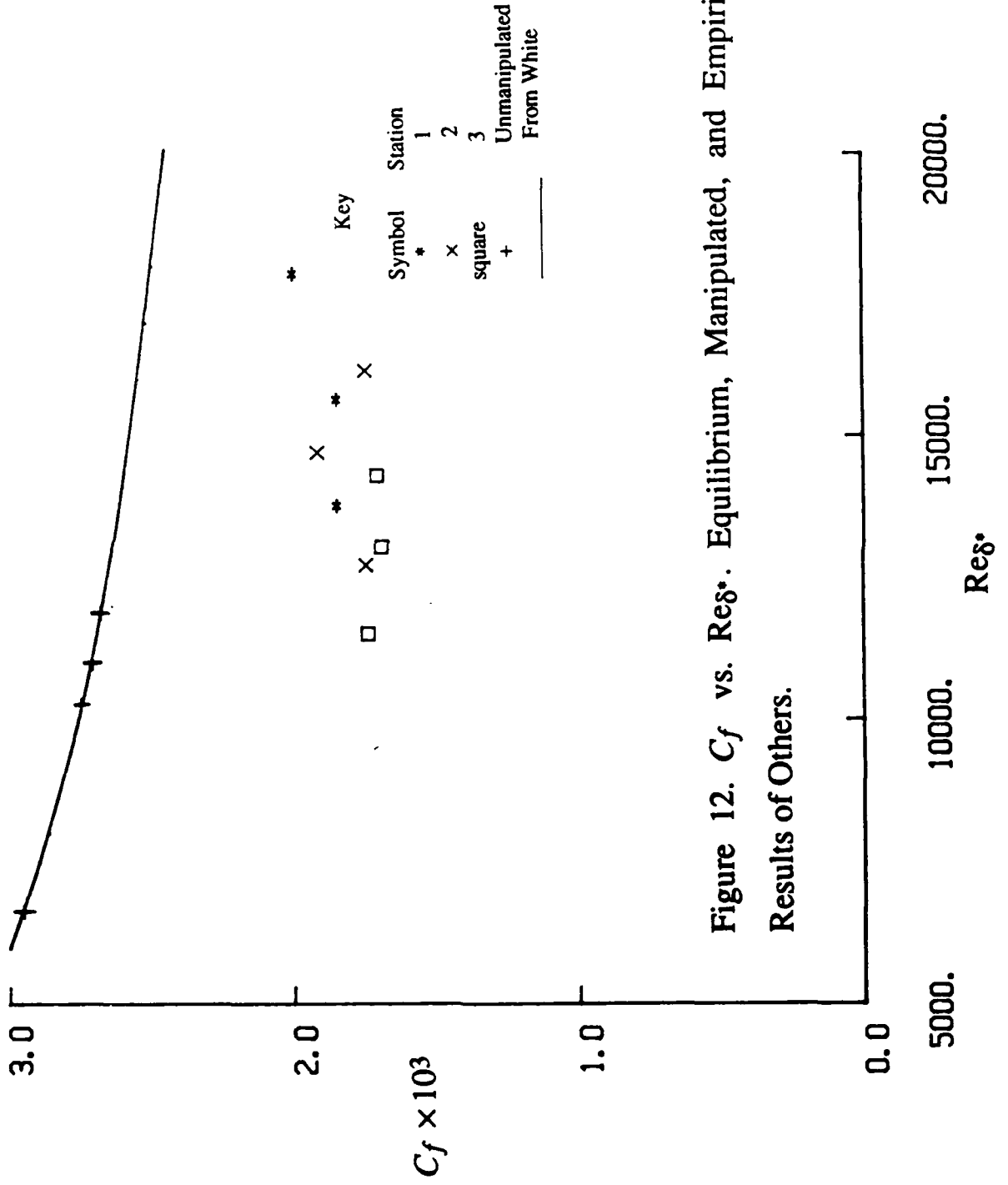
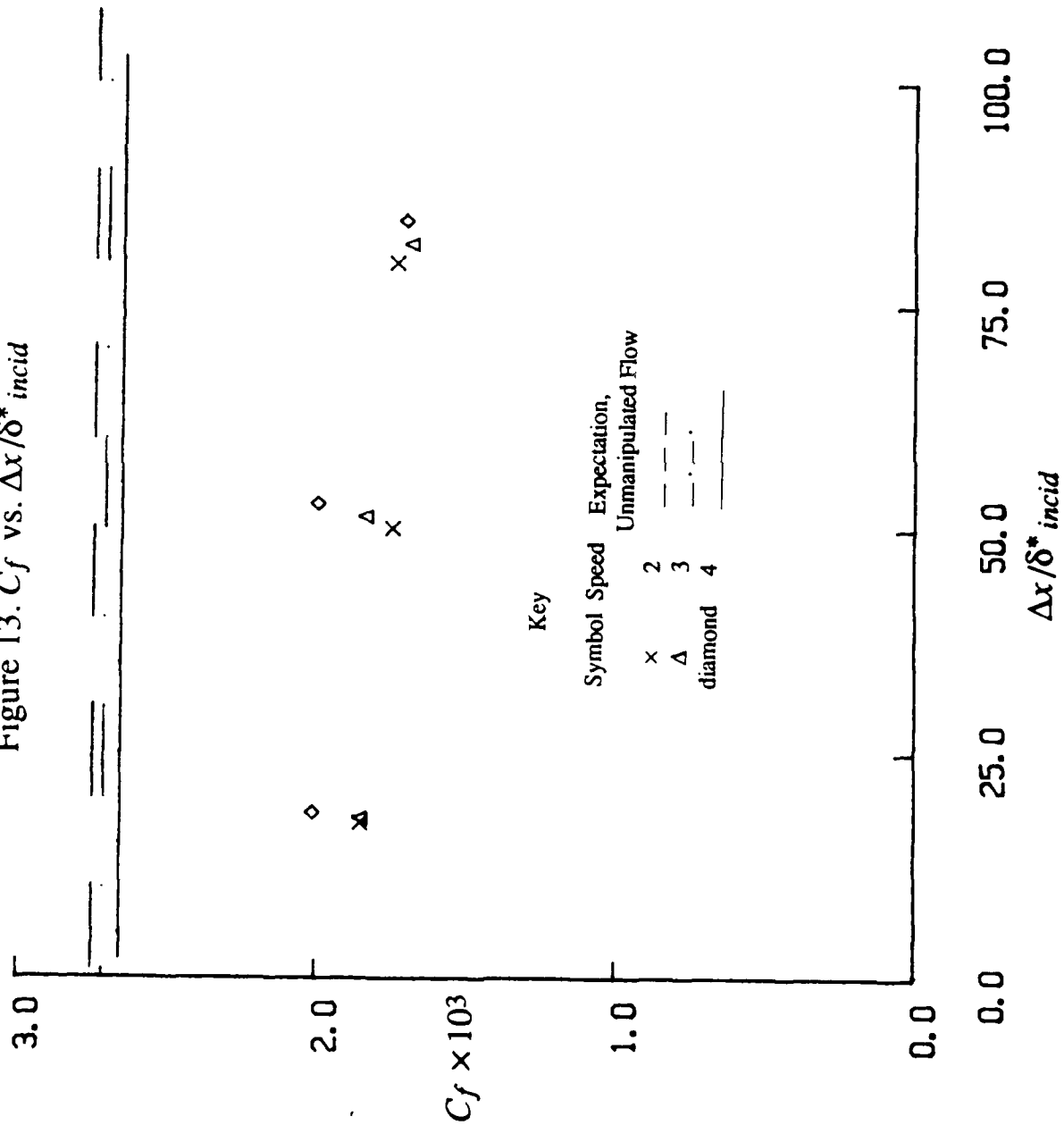
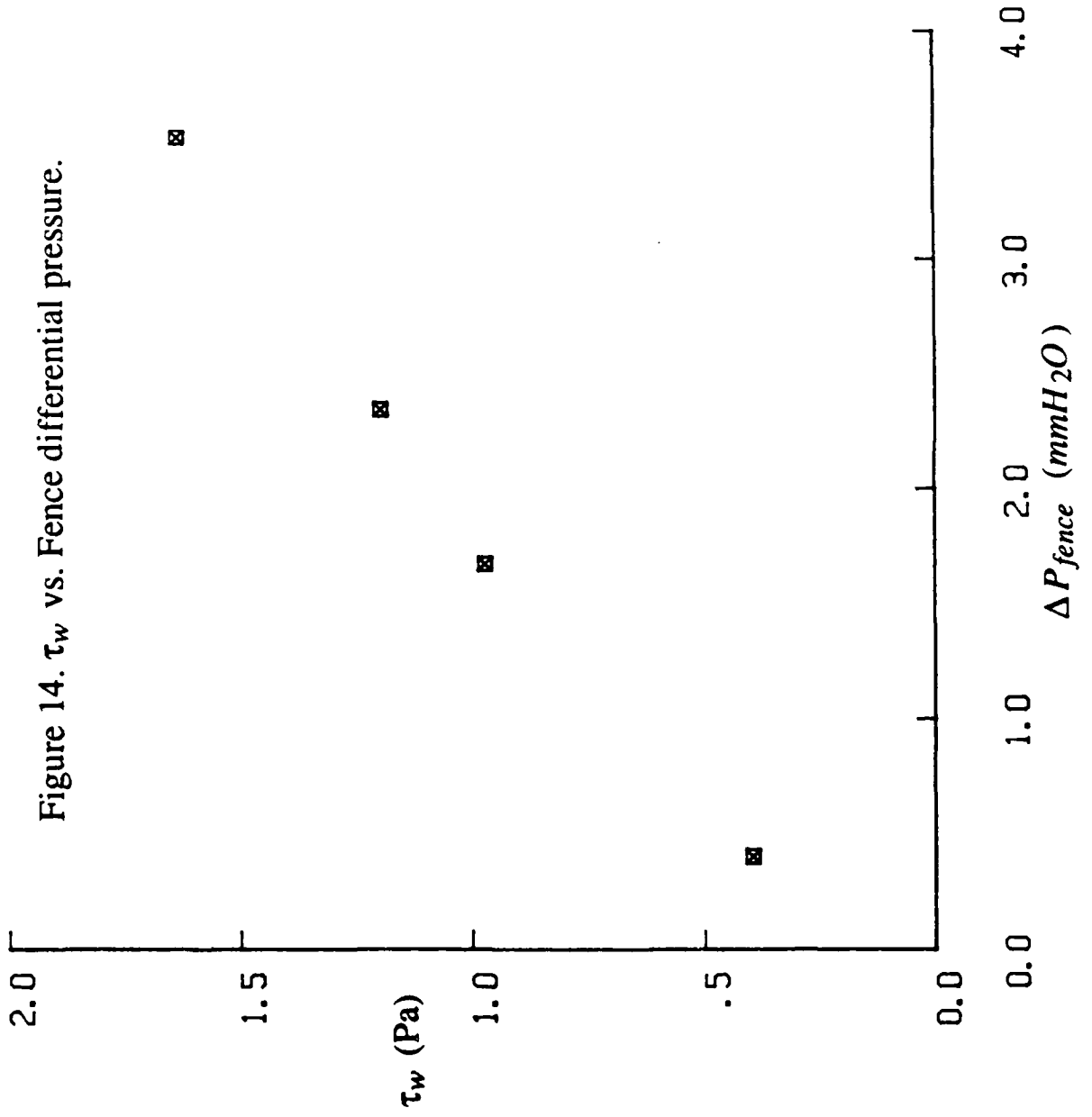


Figure 12. C_f vs. Re_δ . Equilibrium, Manipulated, and Empirical Results of Others.

Figure 13. C_f vs. $\Delta x / \delta^*$ incid





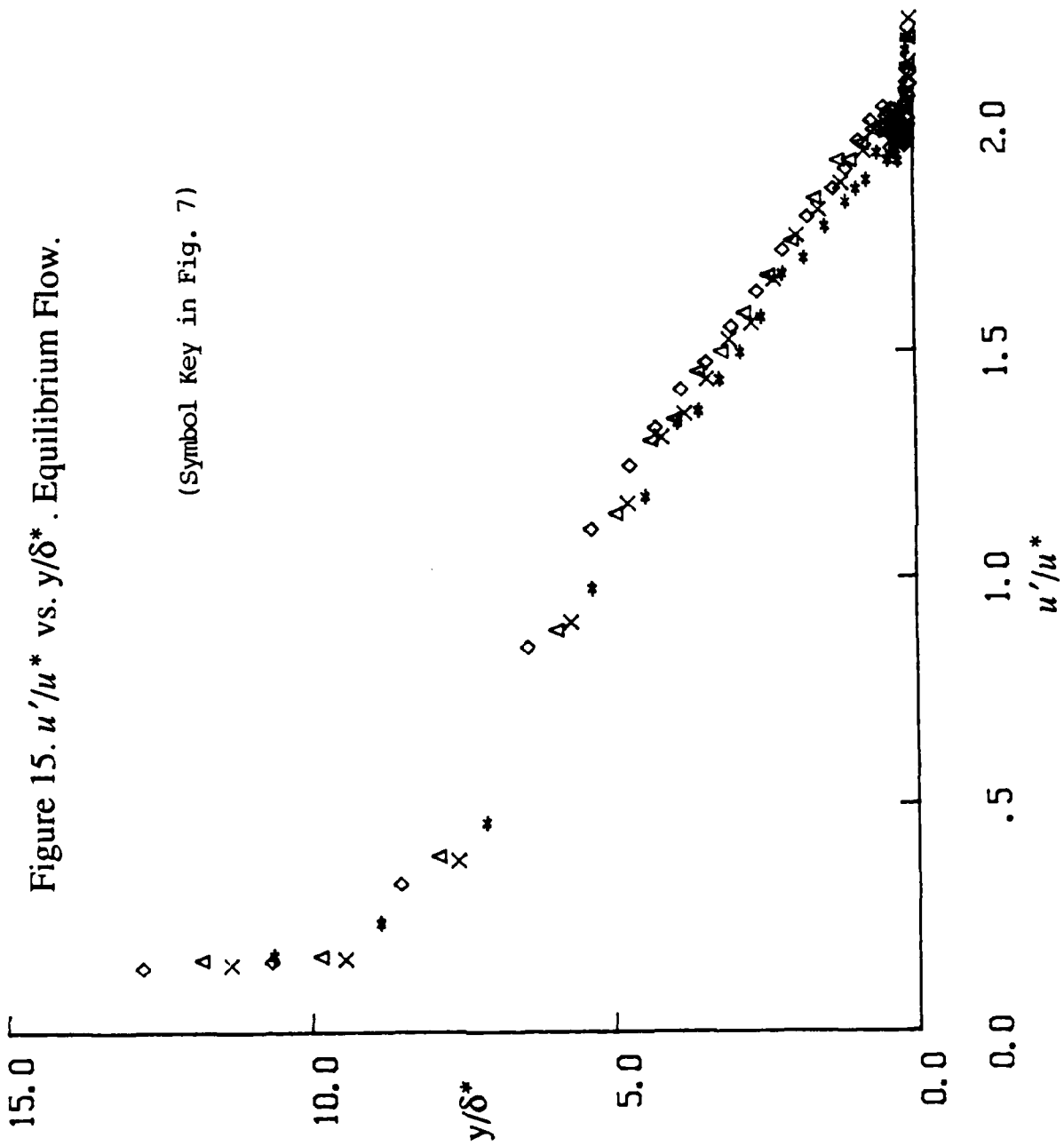


Figure 16a. u'/u^* vs. y/δ^* . Manipulated Flow. Station 1.

(Symbol Key in Fig. 9a)

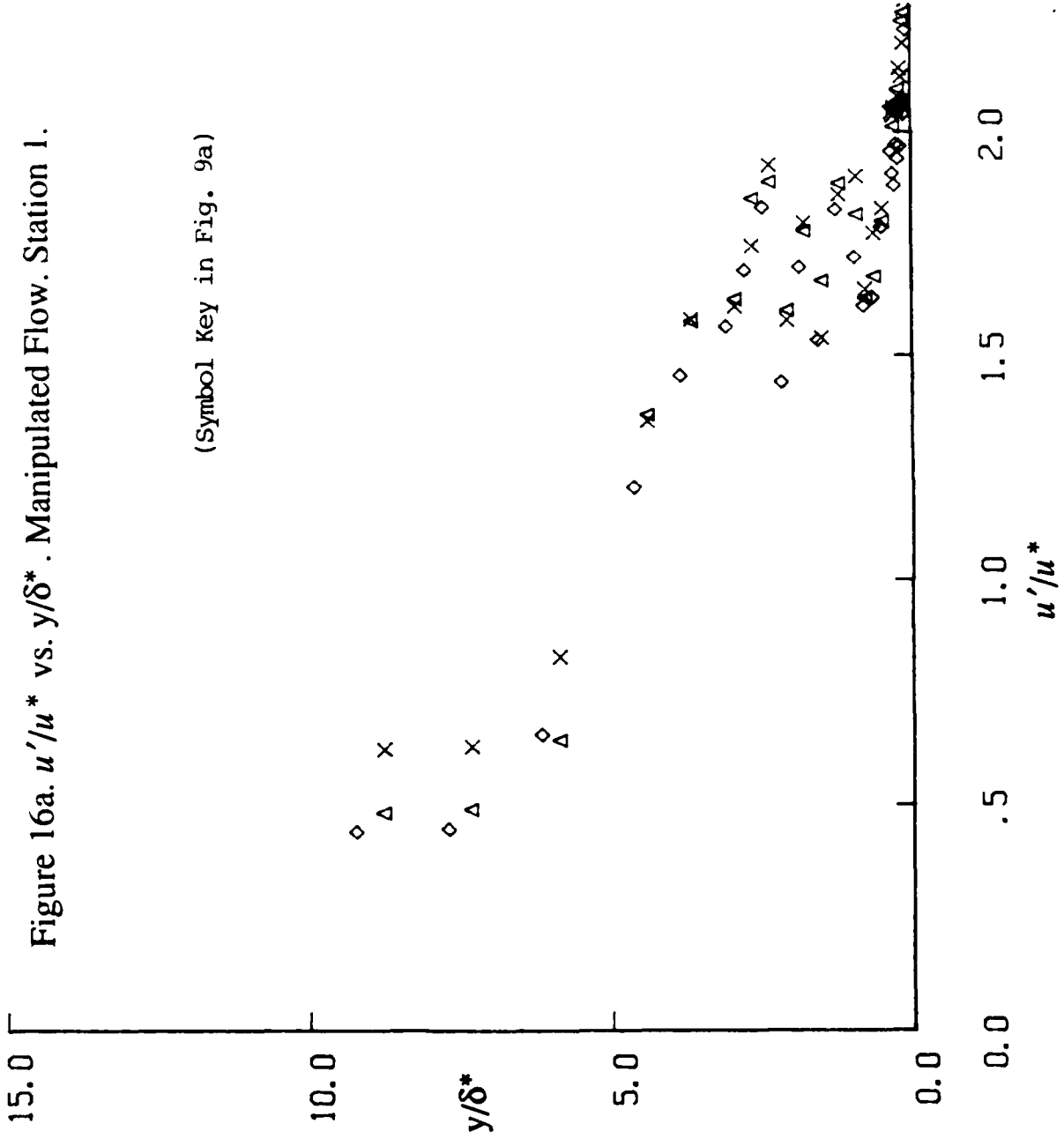
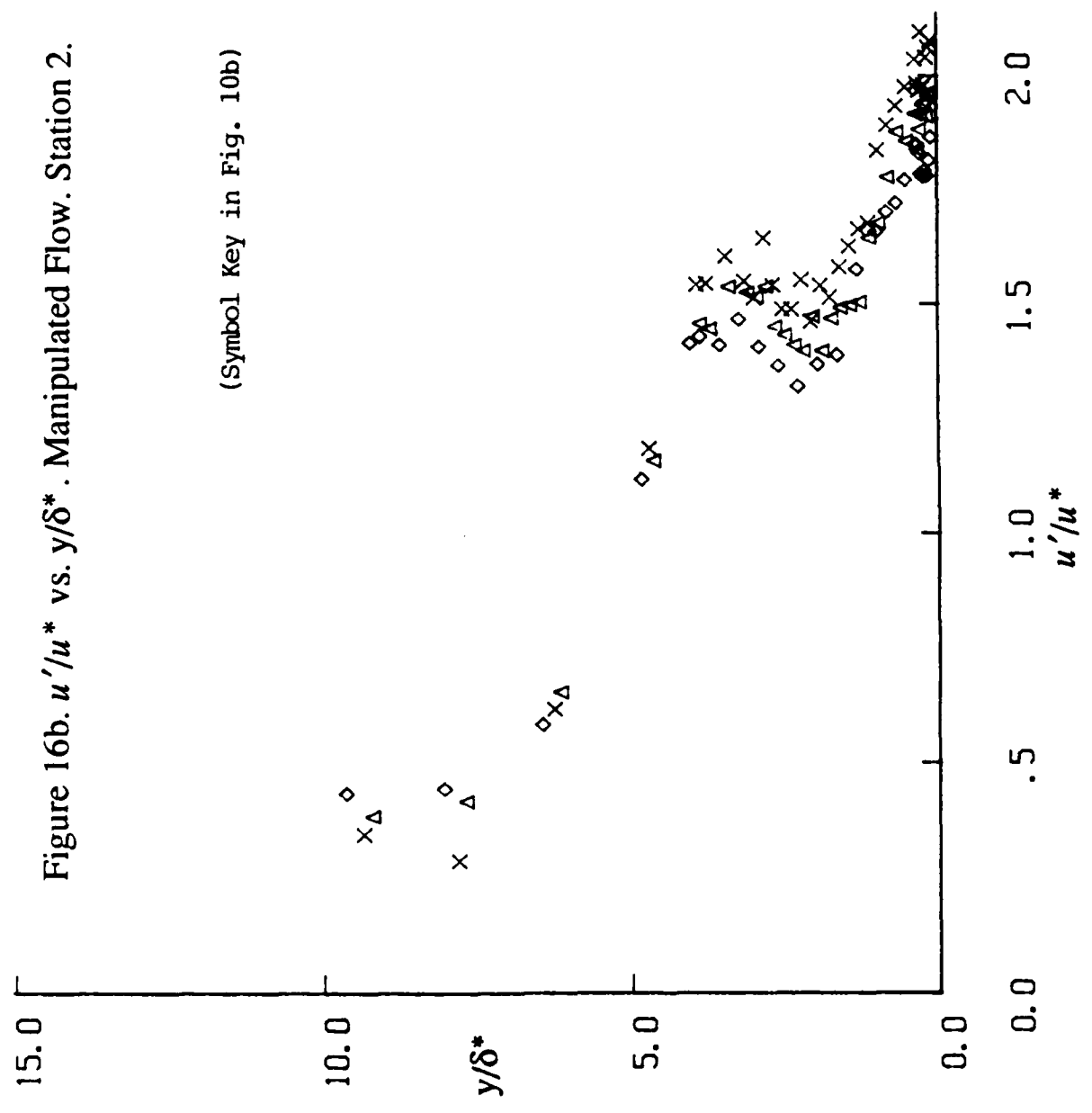


Figure 16b. u'/u^* vs. y/δ^* . Manipulated Flow. Station 2.

(Symbol Key in Fig. 10b)



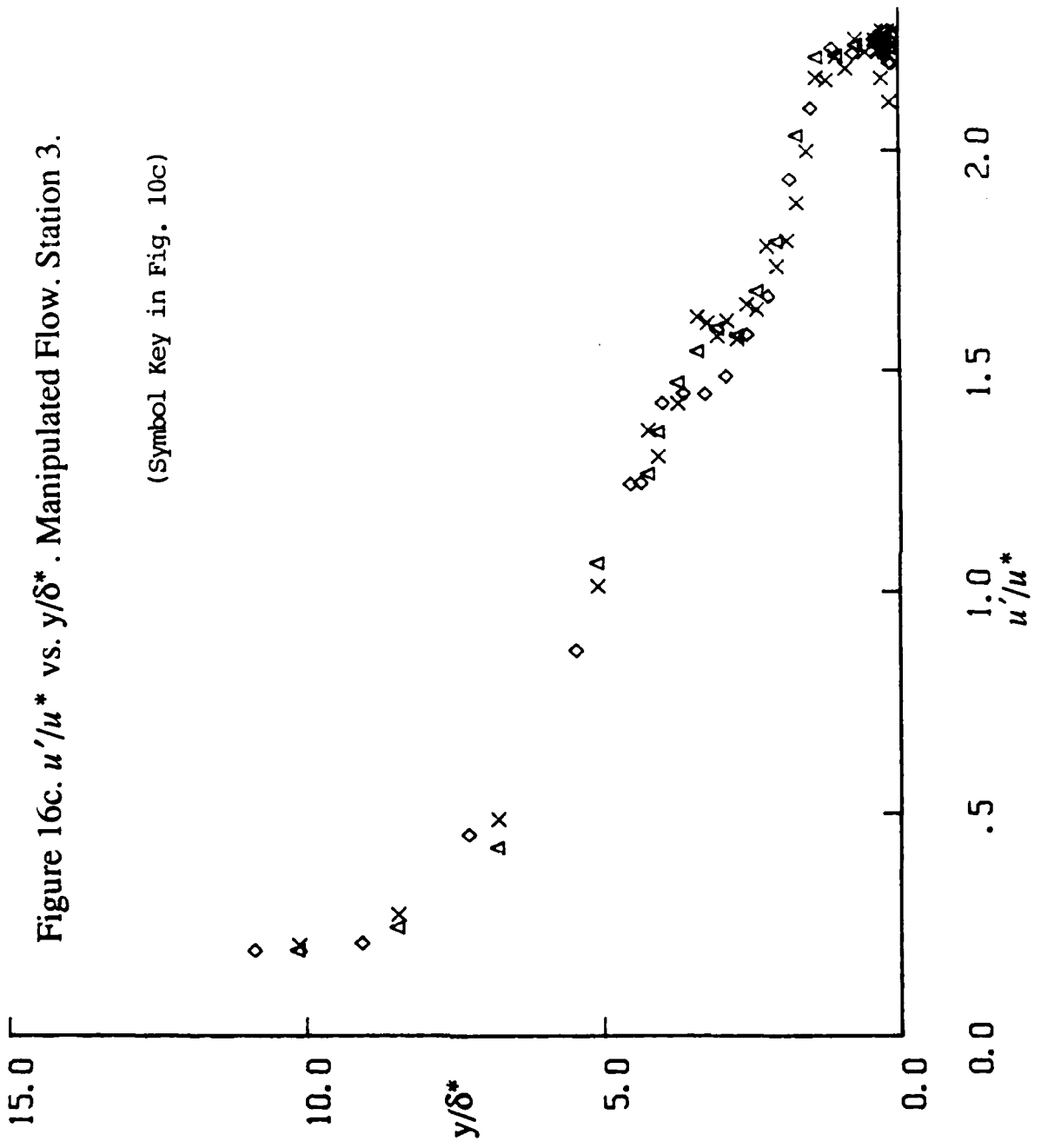


Figure 17a. u'/u^* vs. y/h_c . Manipulated Flow. Station 1.

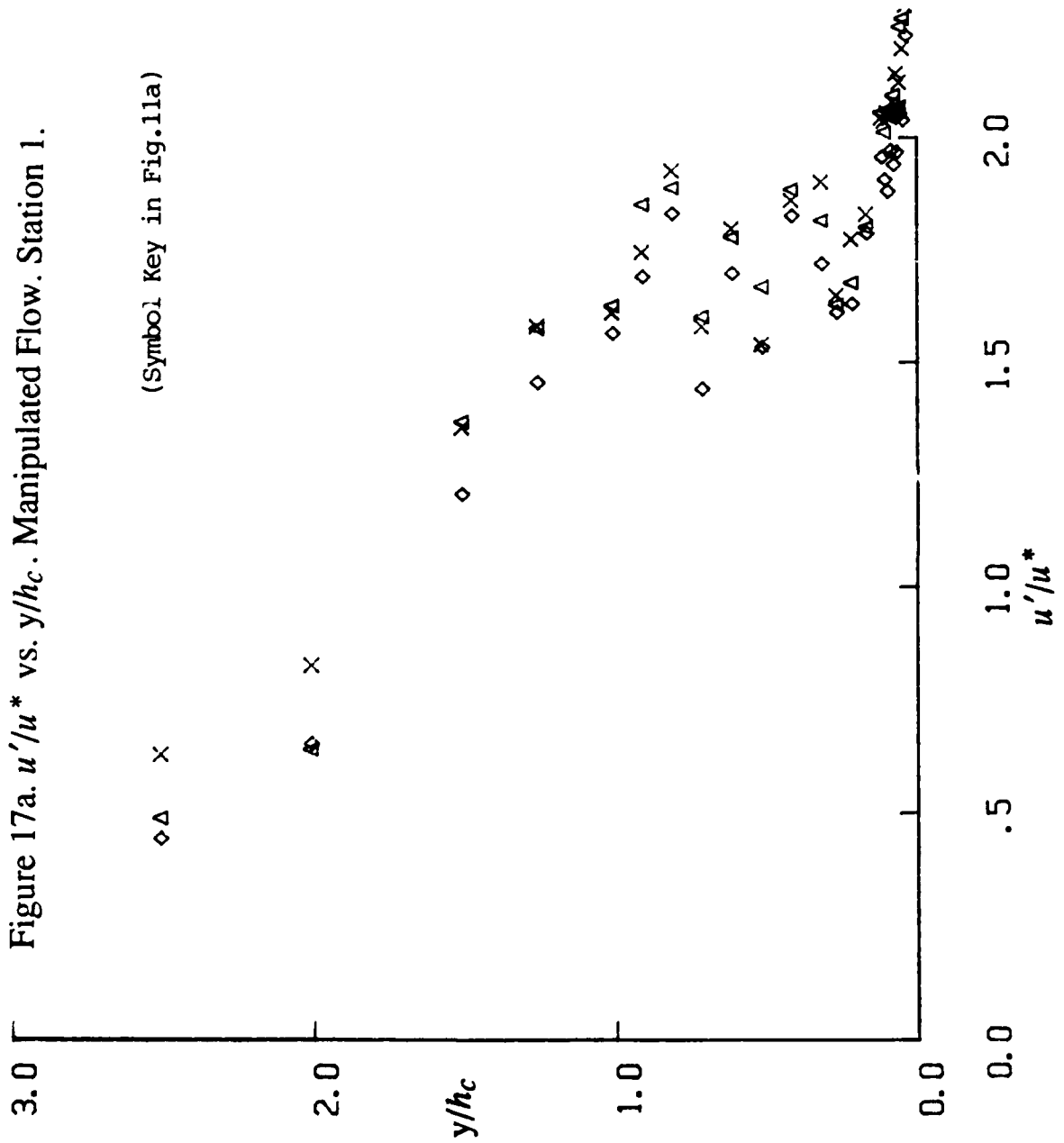
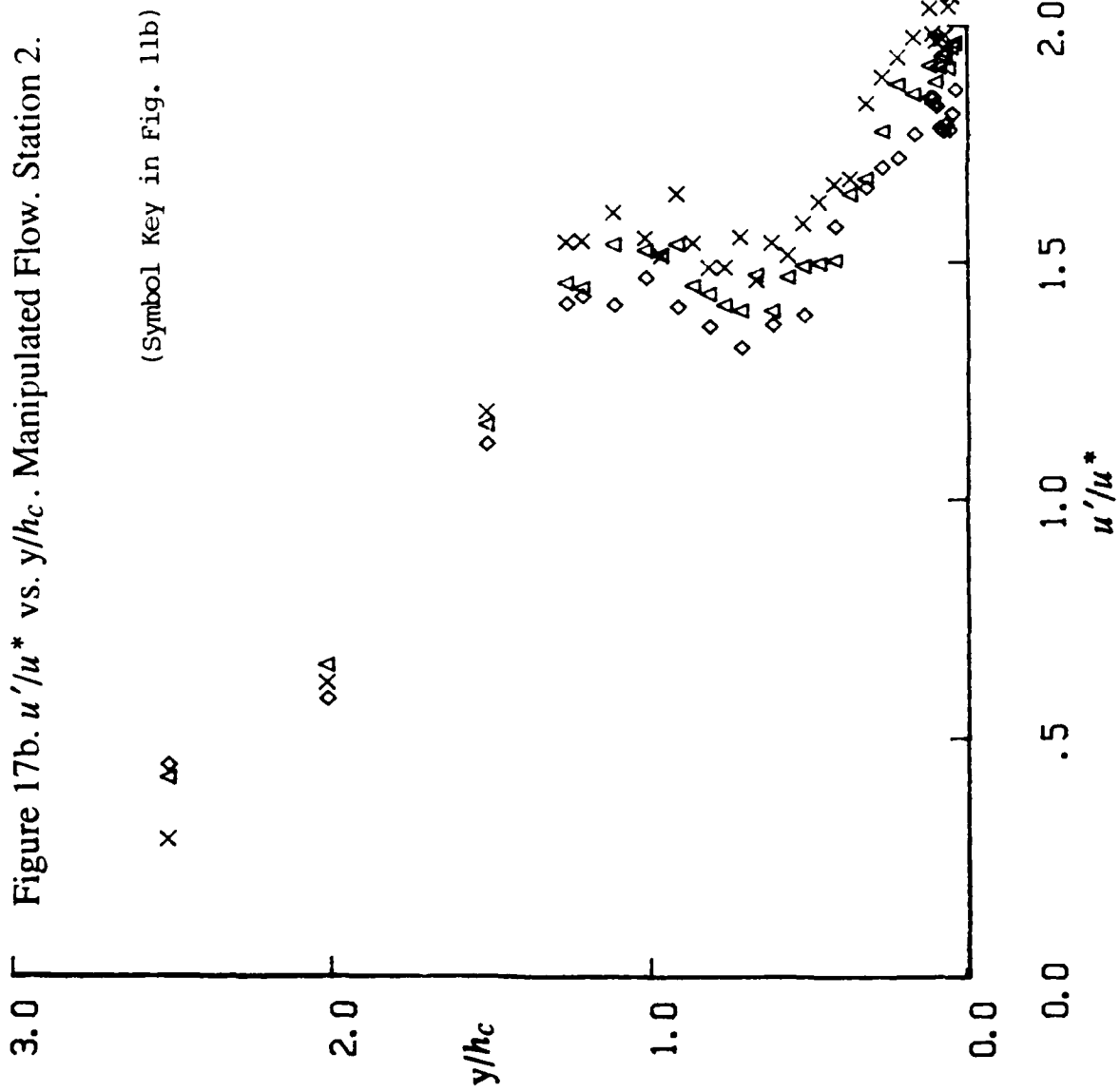
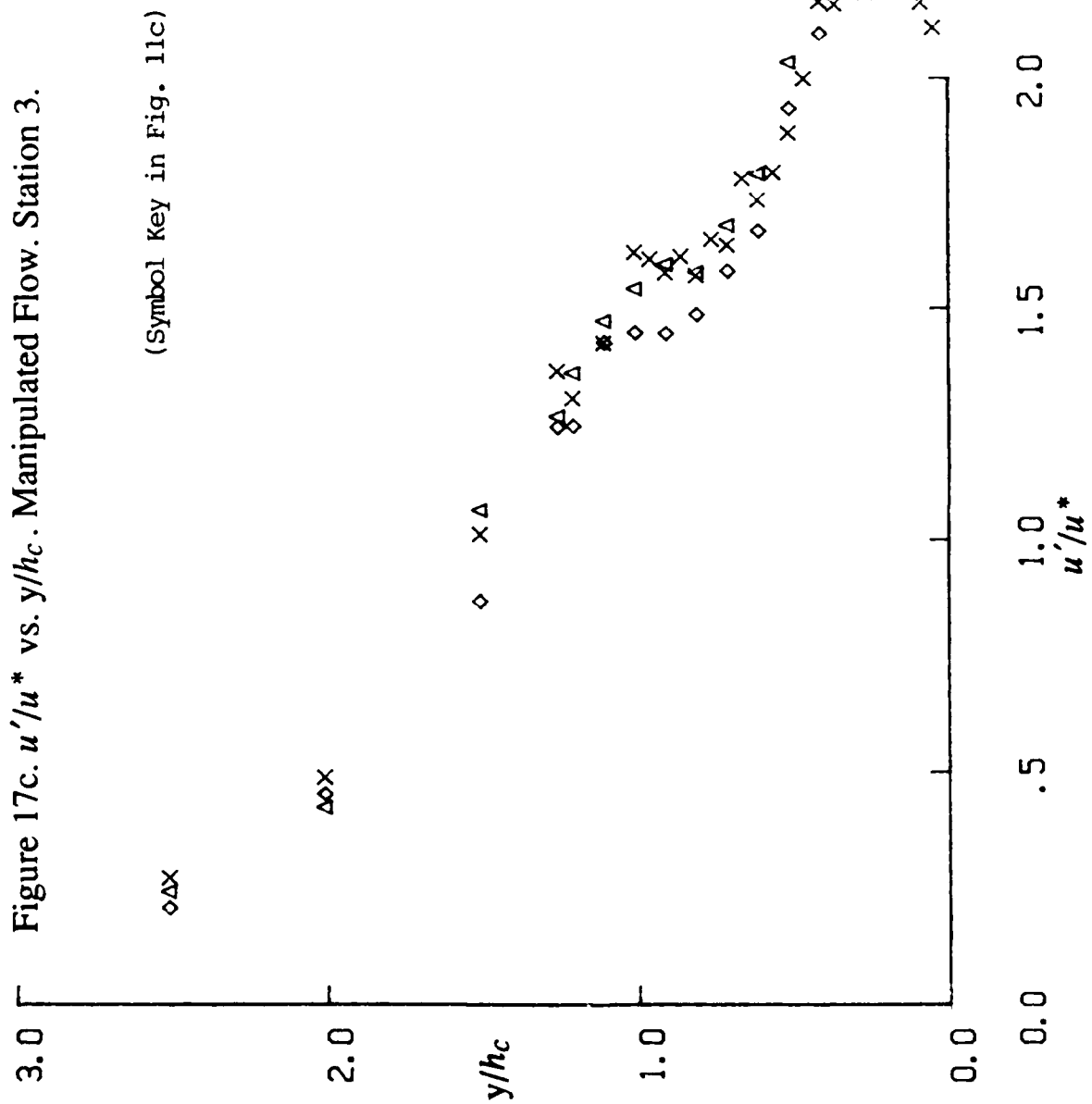


Figure 17b. u'/u^* vs. y/h_c . Manipulated Flow. Station 2.





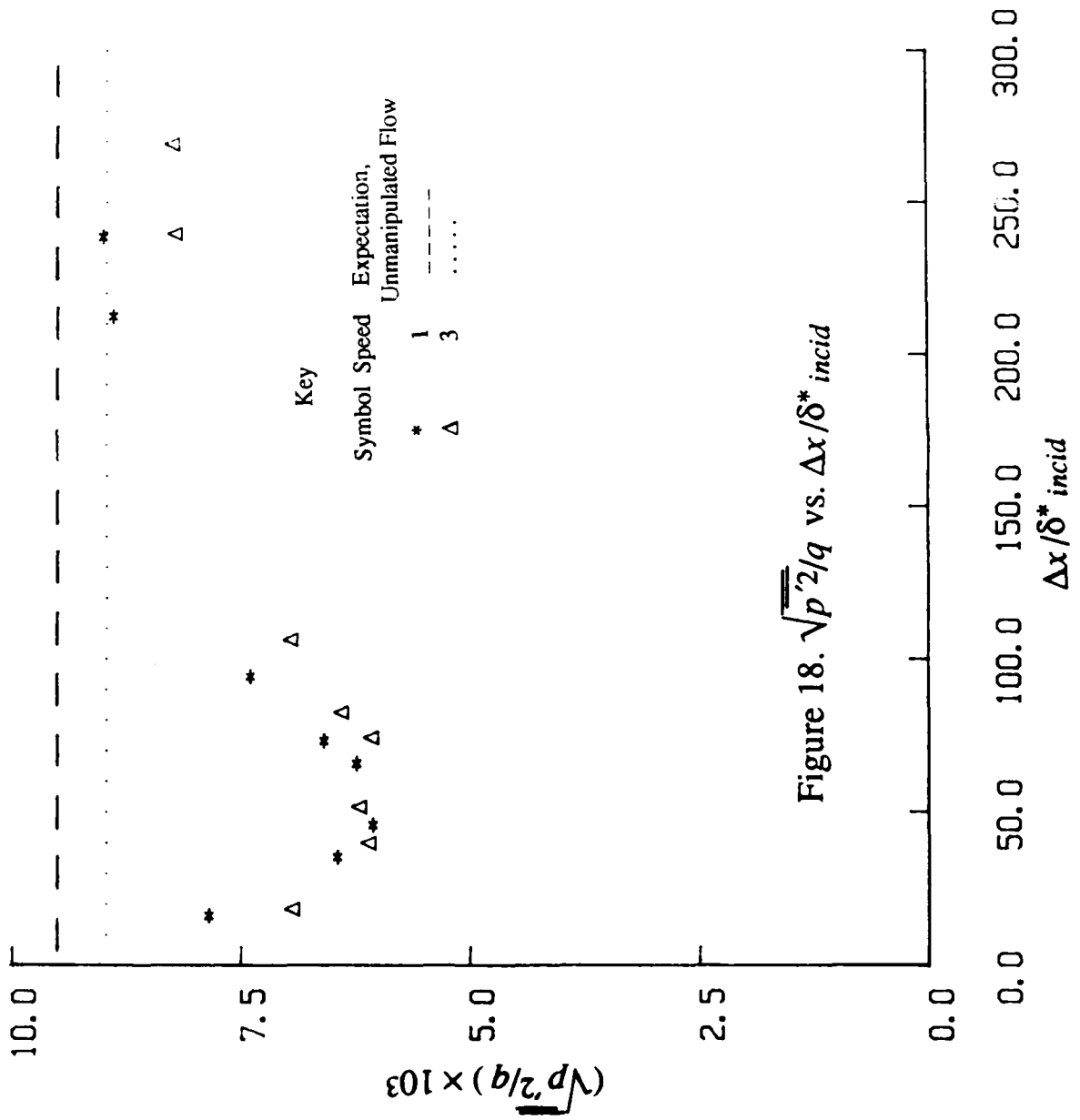


Figure 18. $\sqrt{p^2/q}$ vs. $\Delta x / \delta^* \text{ incid}$

Figure 19. Point Pressure Spectra. Equilibrium Flow. Outer-Inner Vari-

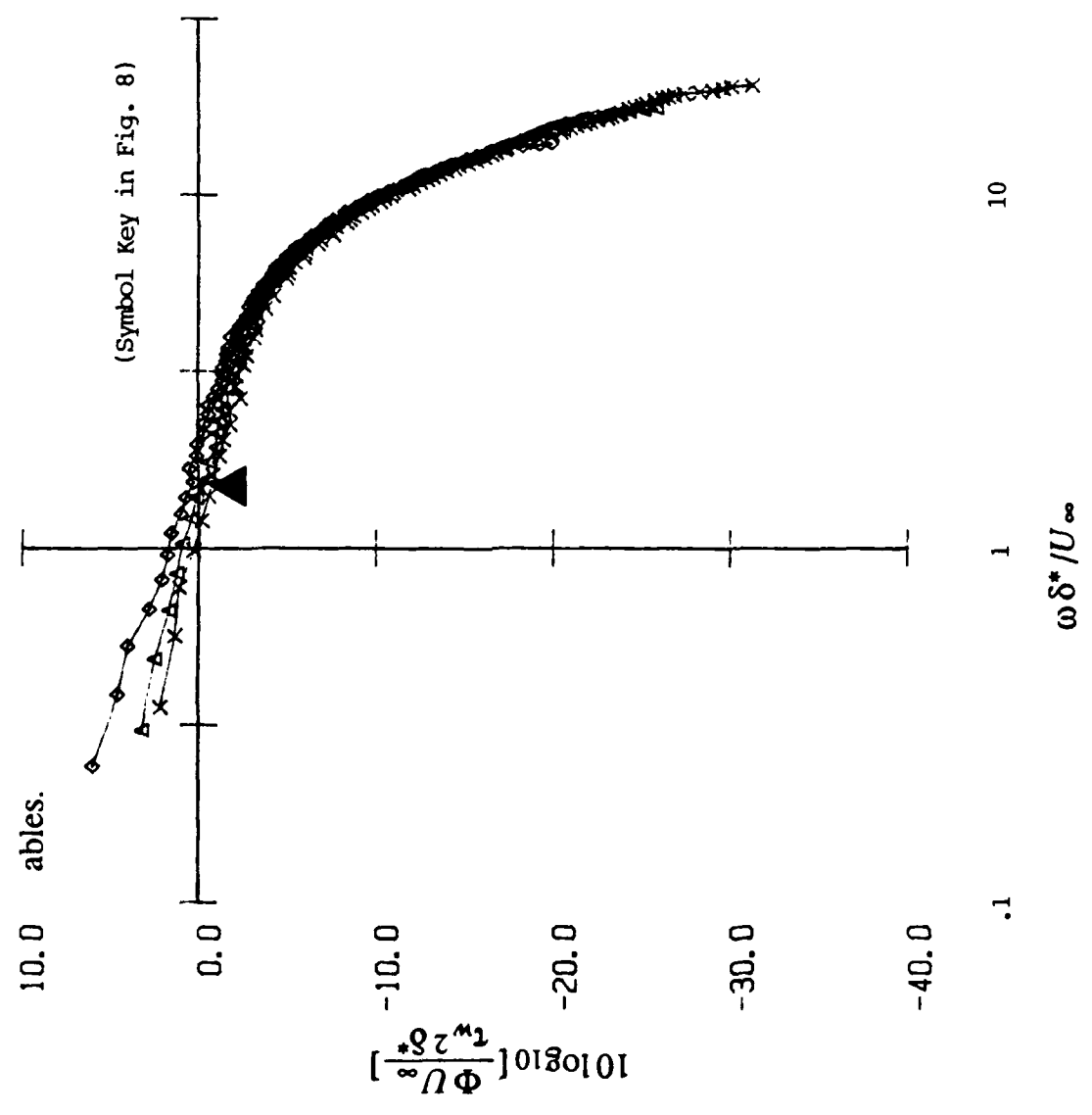


Figure 20a. Point Pressure Spectra. Manipulated Flow. Outer-Inner Variables. Station 1.

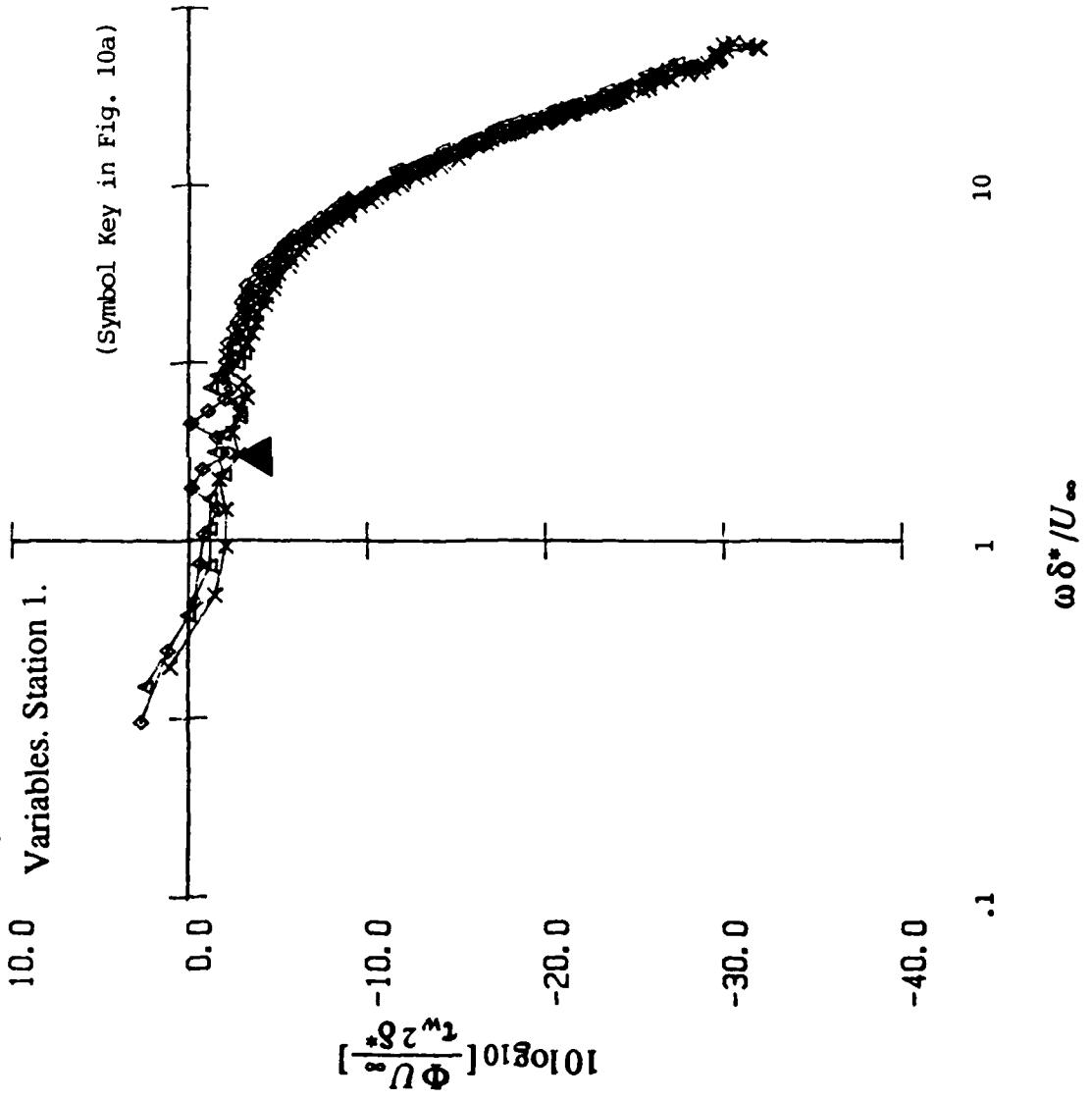


Figure 20b. Point Pressure Spectra. Manipulated Flow. Outer-Inner Variables. Station 2.

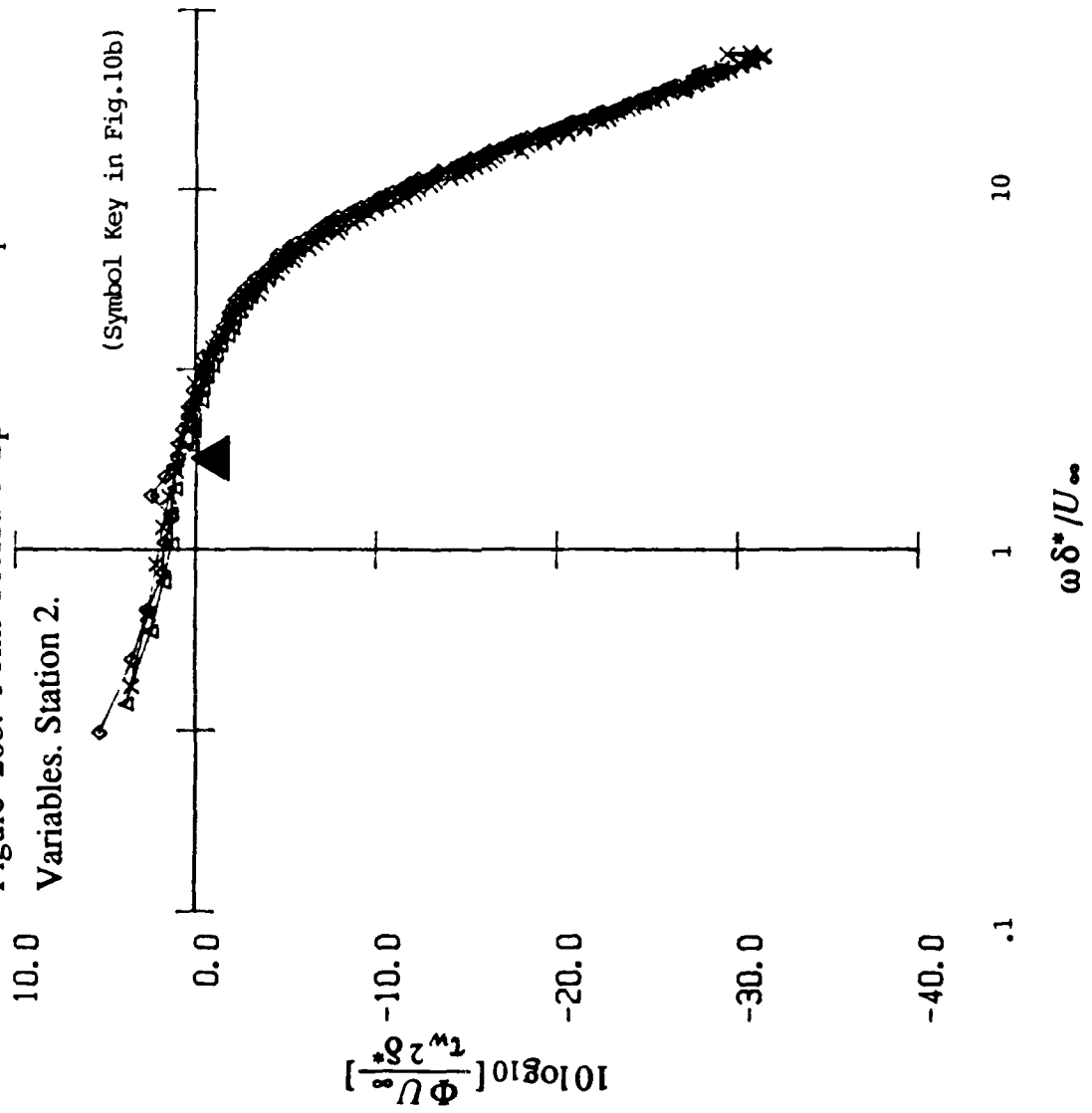


Figure 20c. Point Pressure Spectra. Manipulated Flow. Outer-Inner Variables. Station 3.

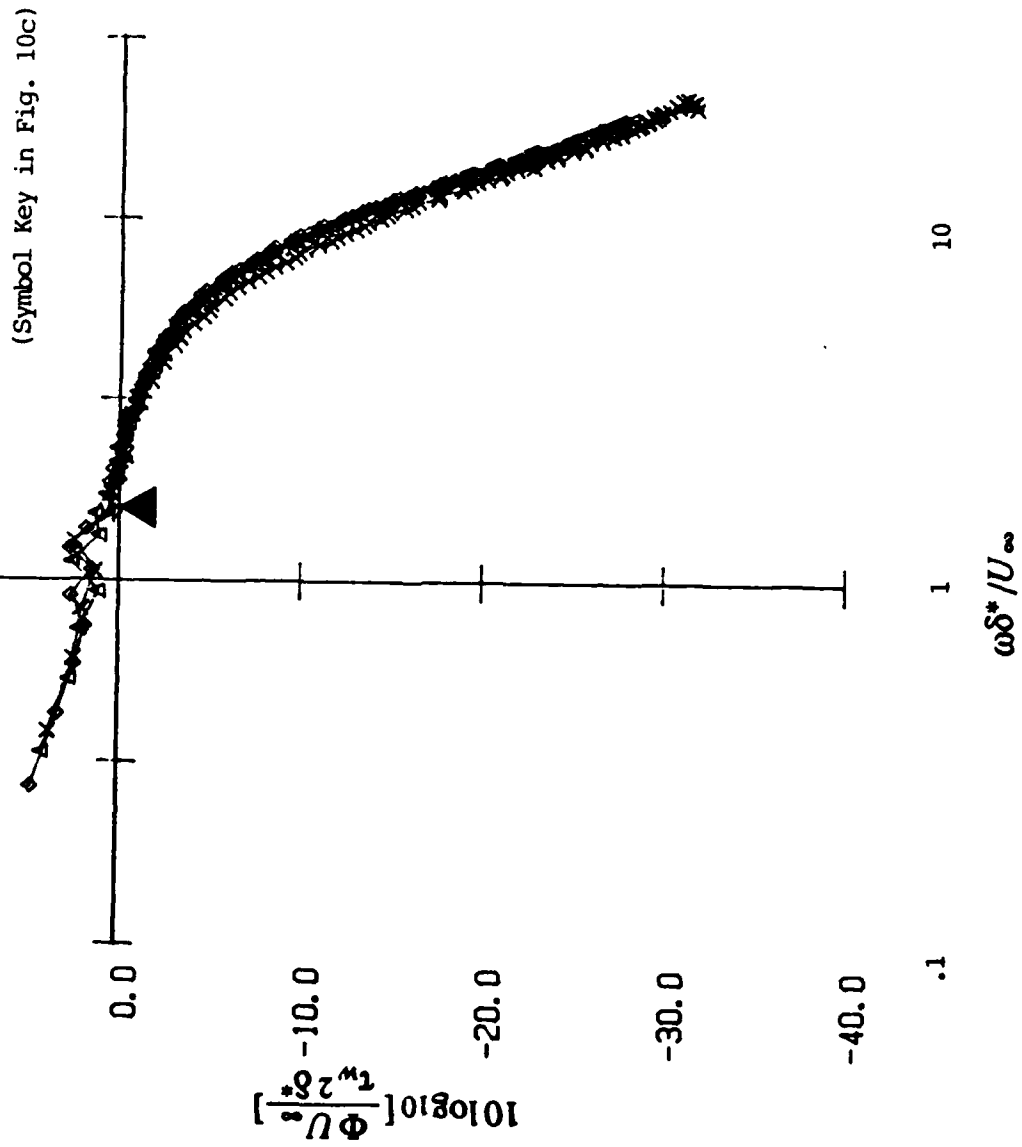


Figure 21. Point Pressure Spectra. Equilibrium Flow. Transducer Vari-
ables.

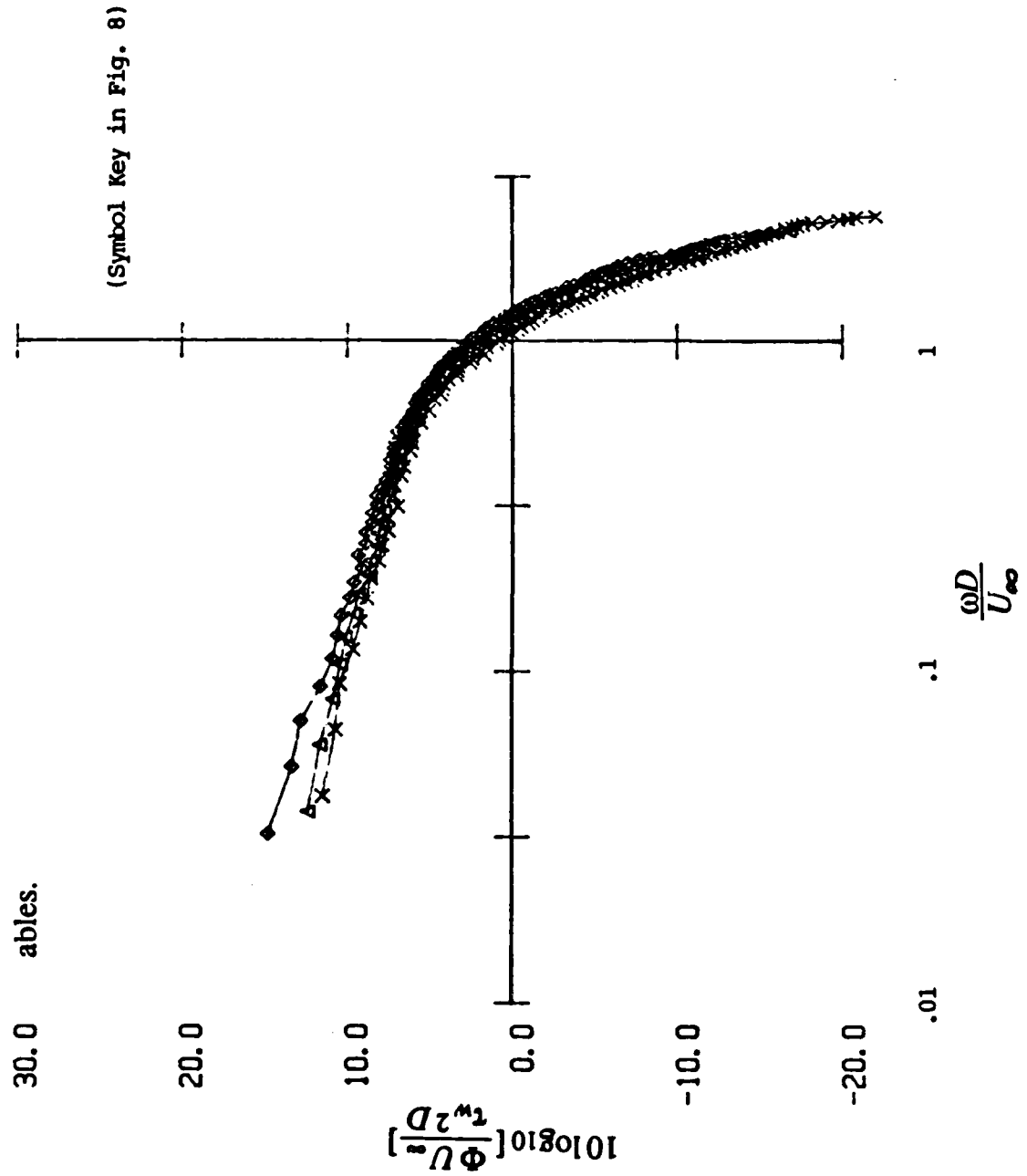


Figure 22a. Point Pressure Spectra. Manipulated Flow. Transducer Variables. Station 1.

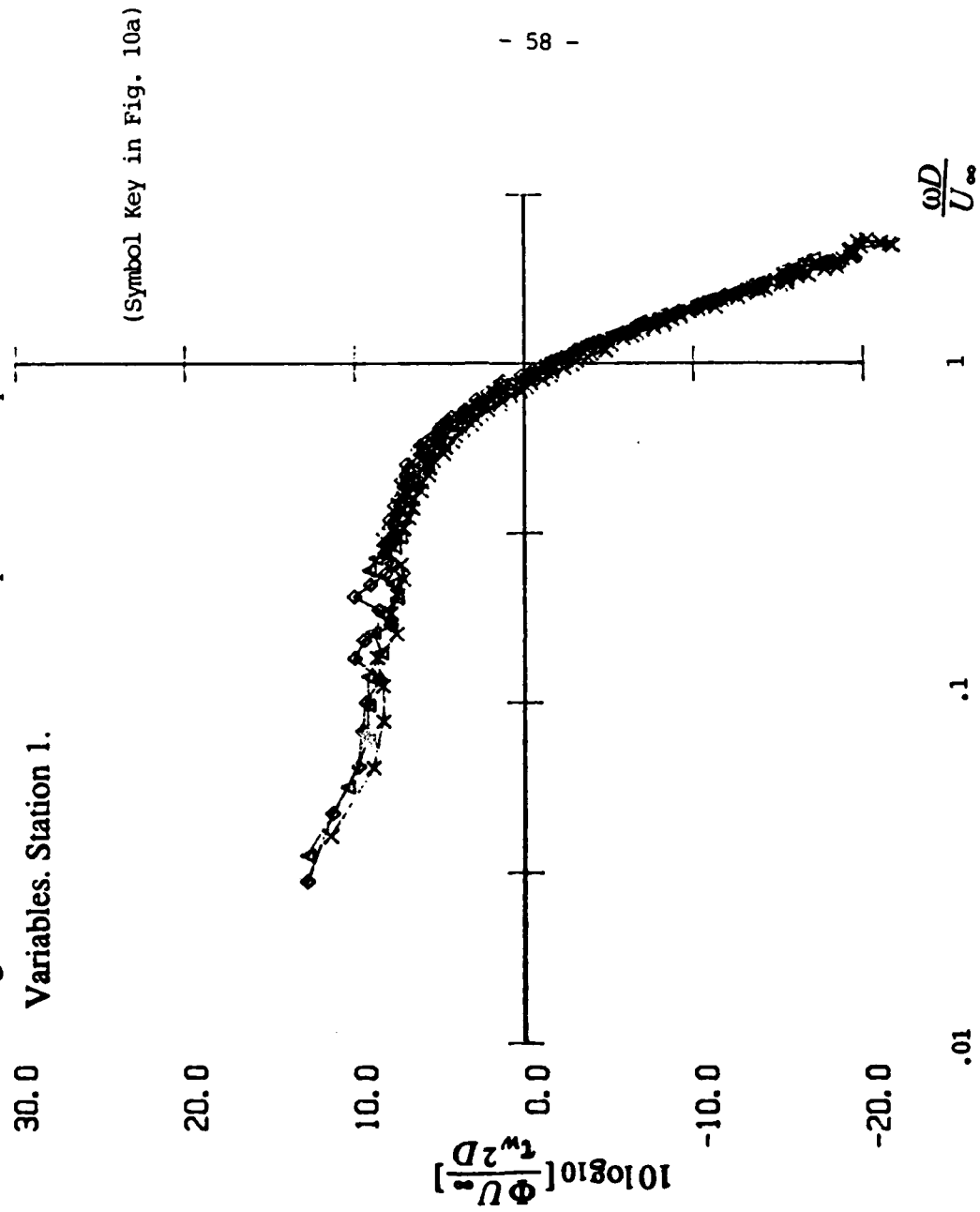


Figure 22b. Point Pressure Spectra. Manipulated Flow. Transducer Variables. Station 2.

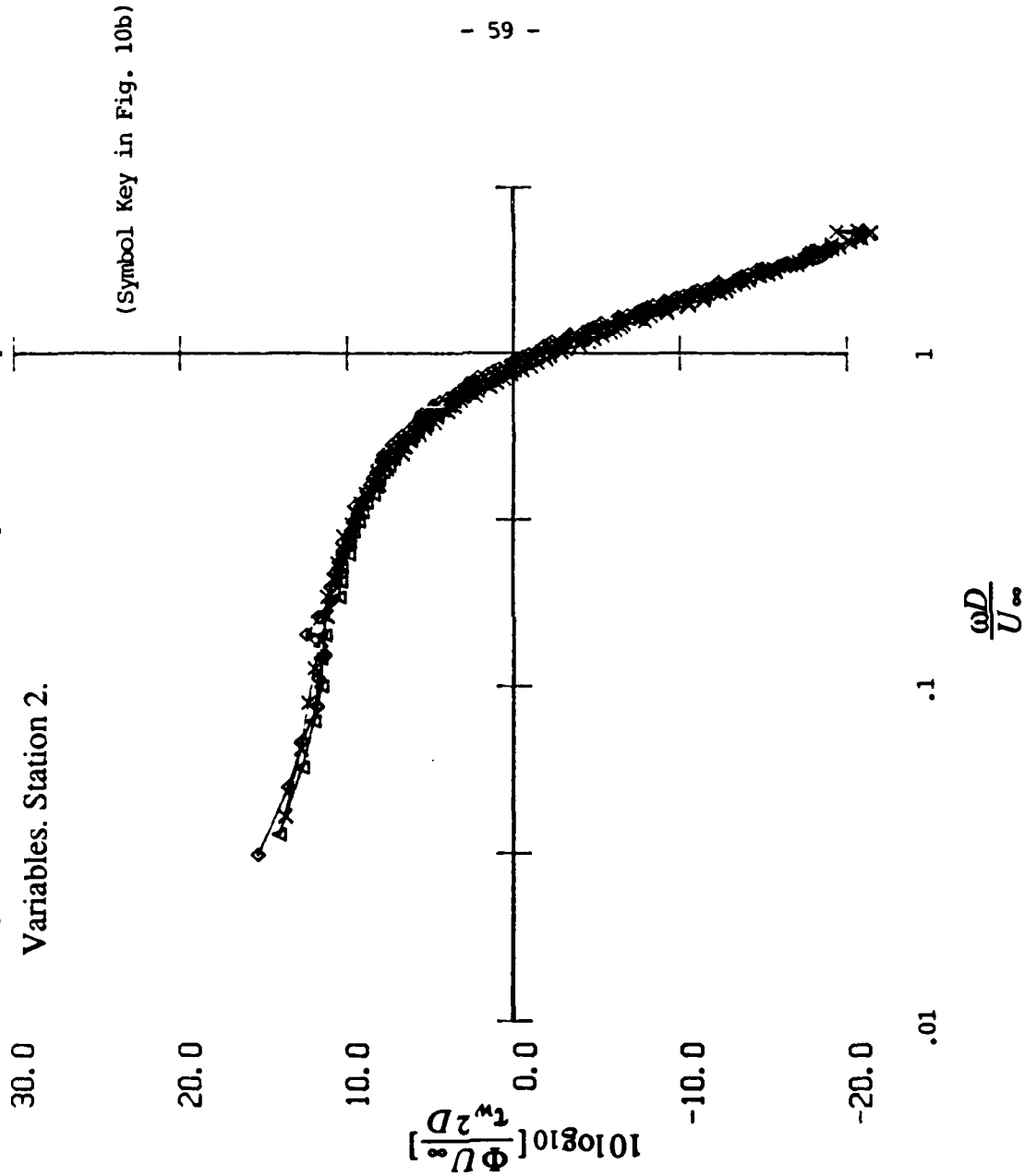
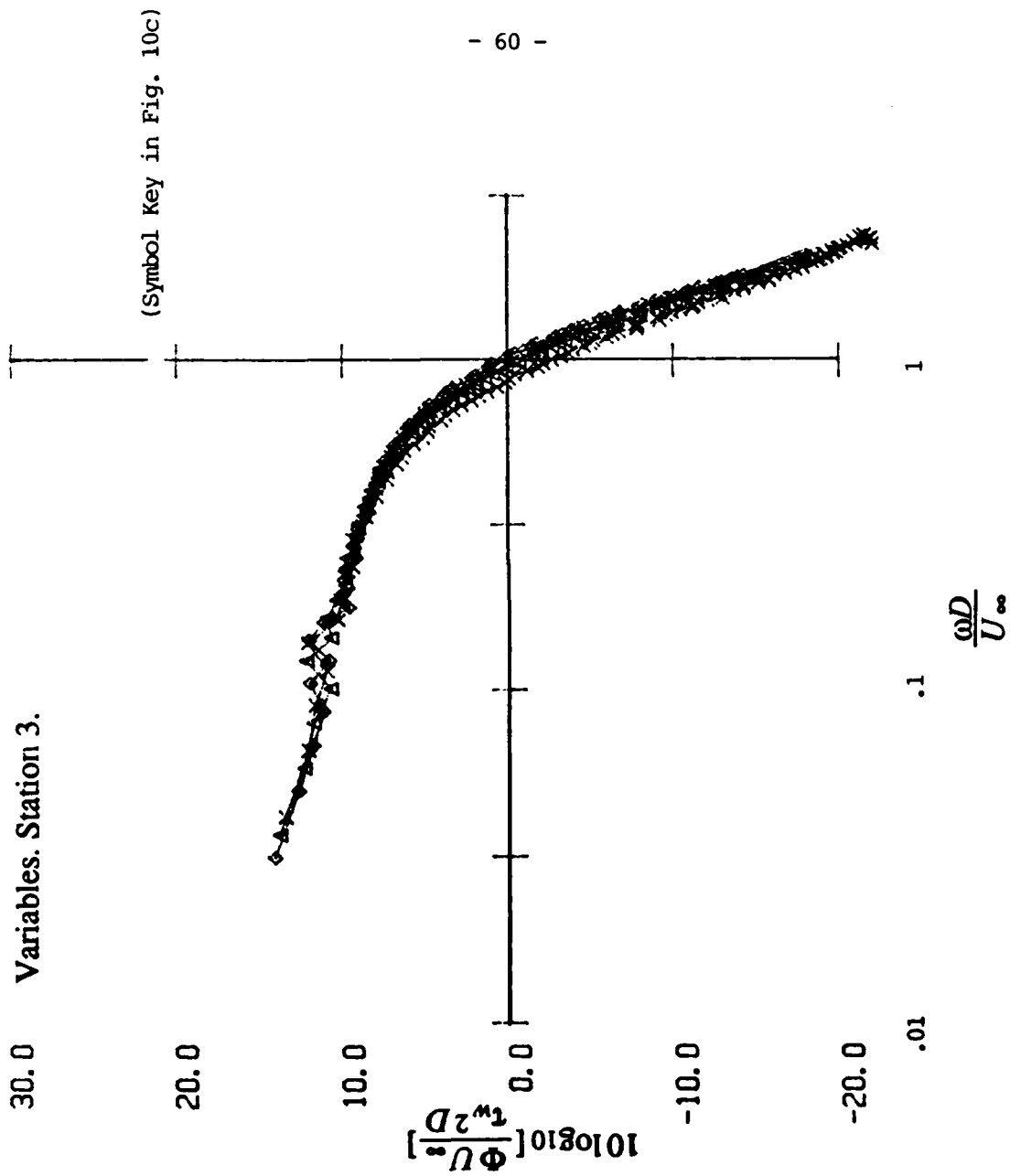
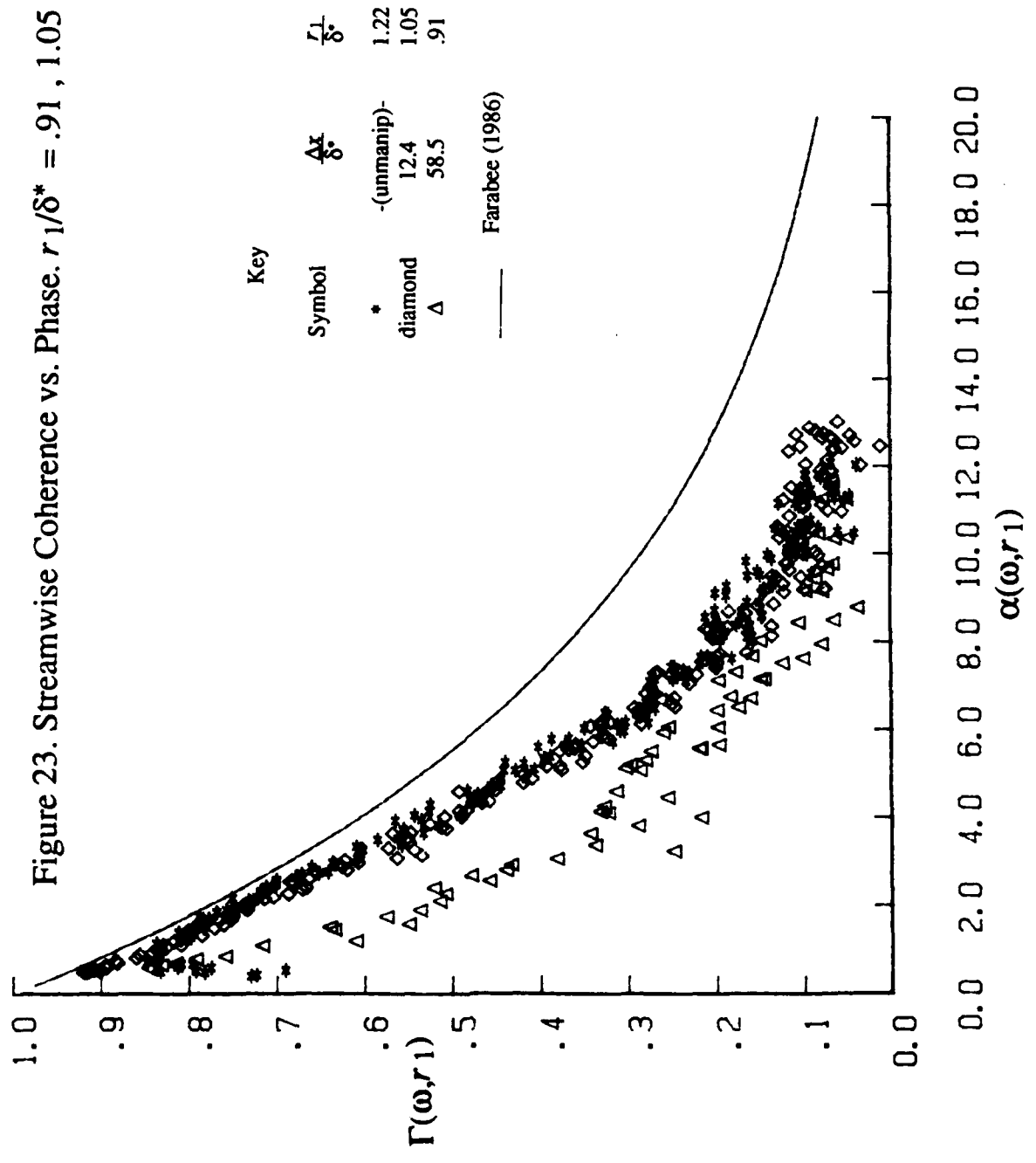
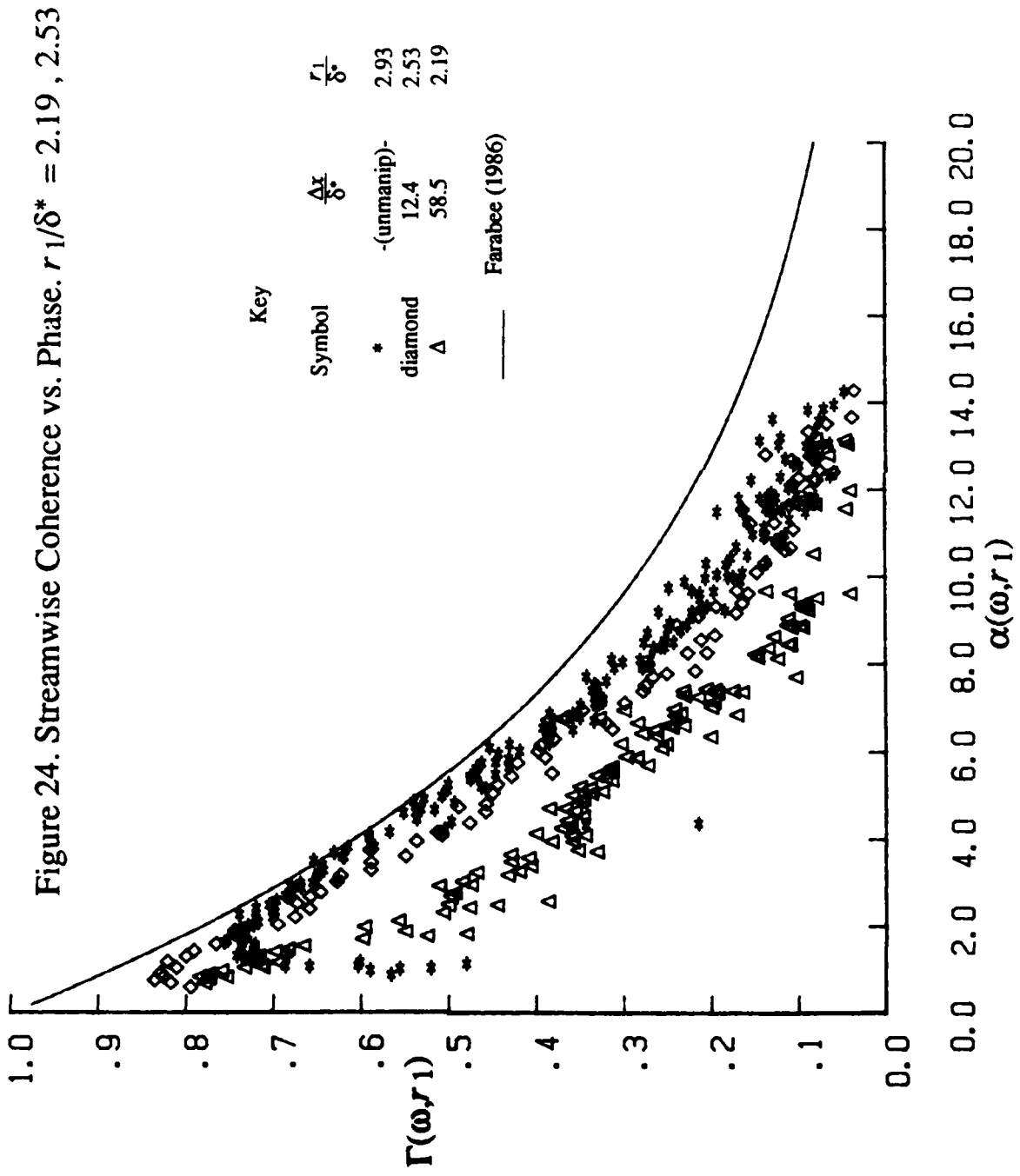
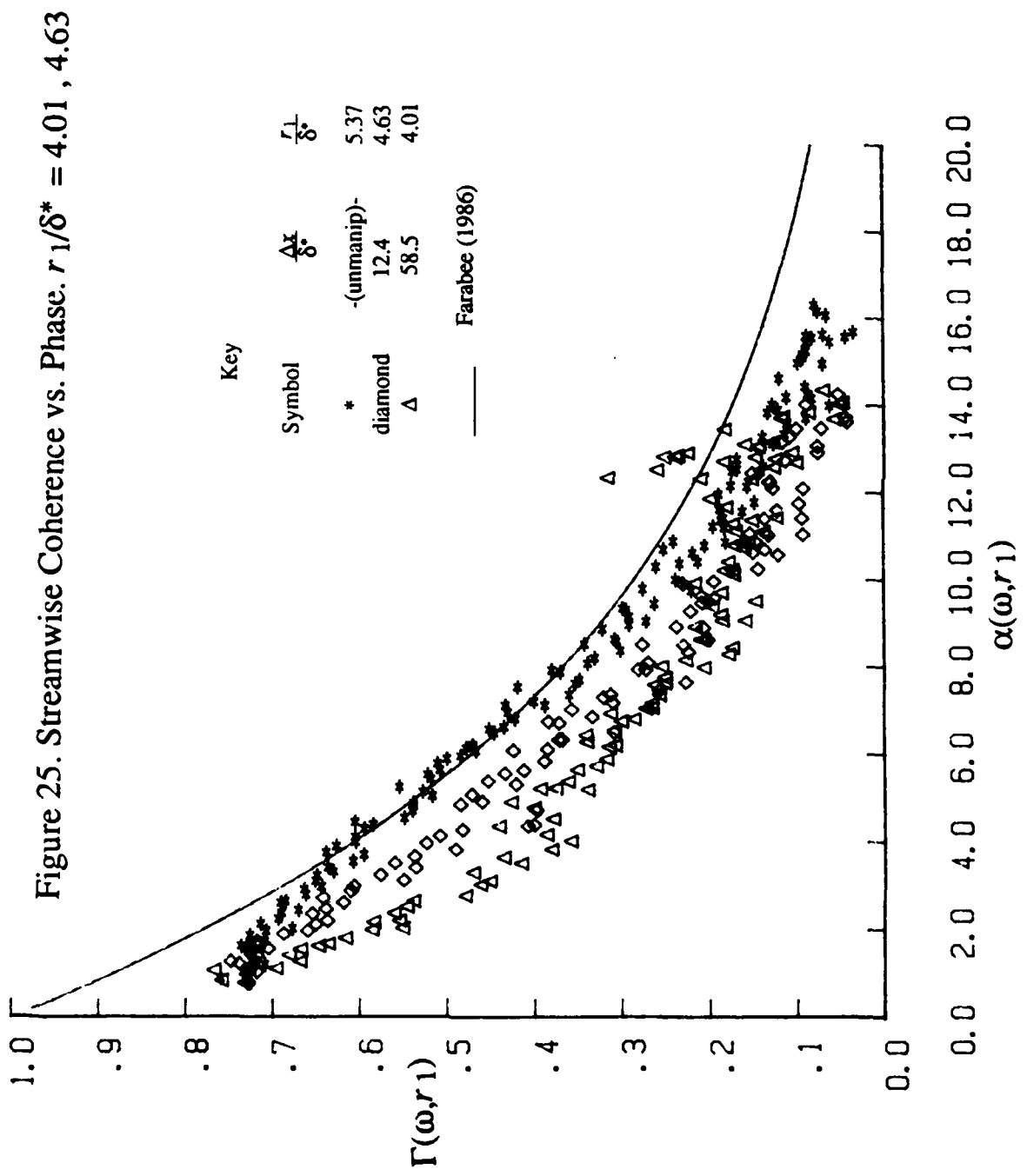


Figure 22c. Point Pressure Spectra. Manipulated Flow. Transducer Variables. Station 3.









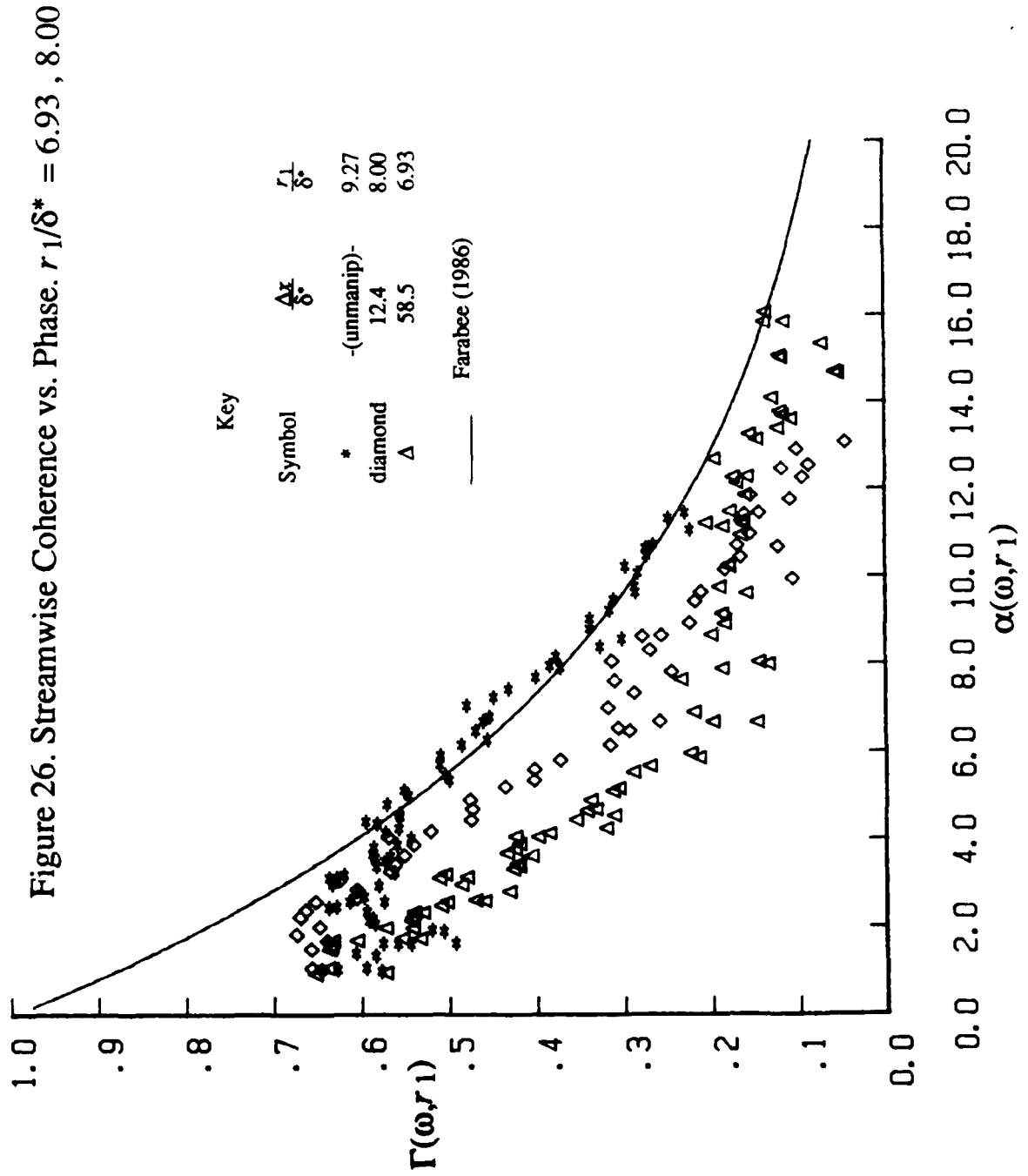
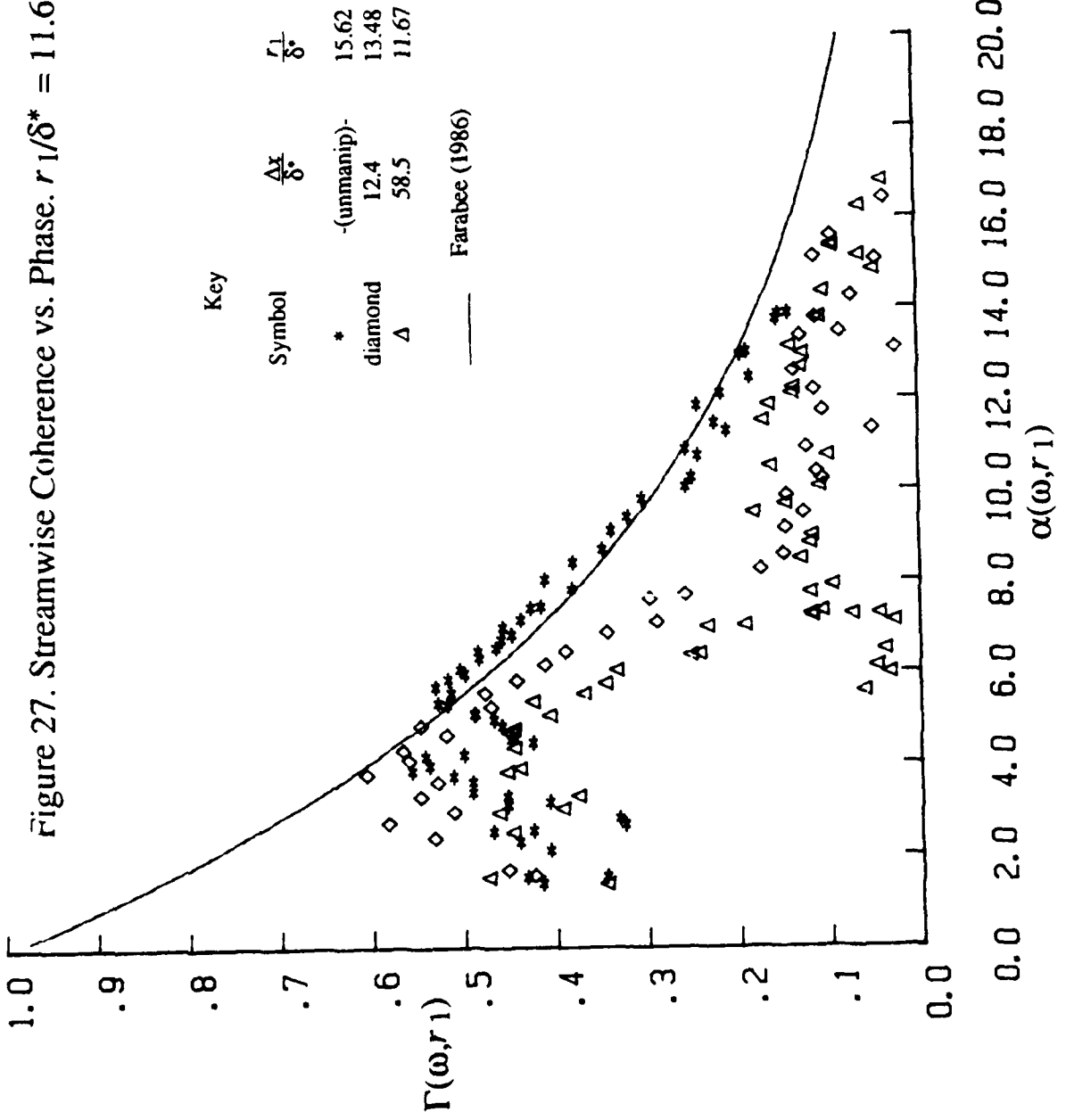


Figure 27. Streamwise Coherence vs. Phase. $r_1/\delta^* = 11.67, 13.48$



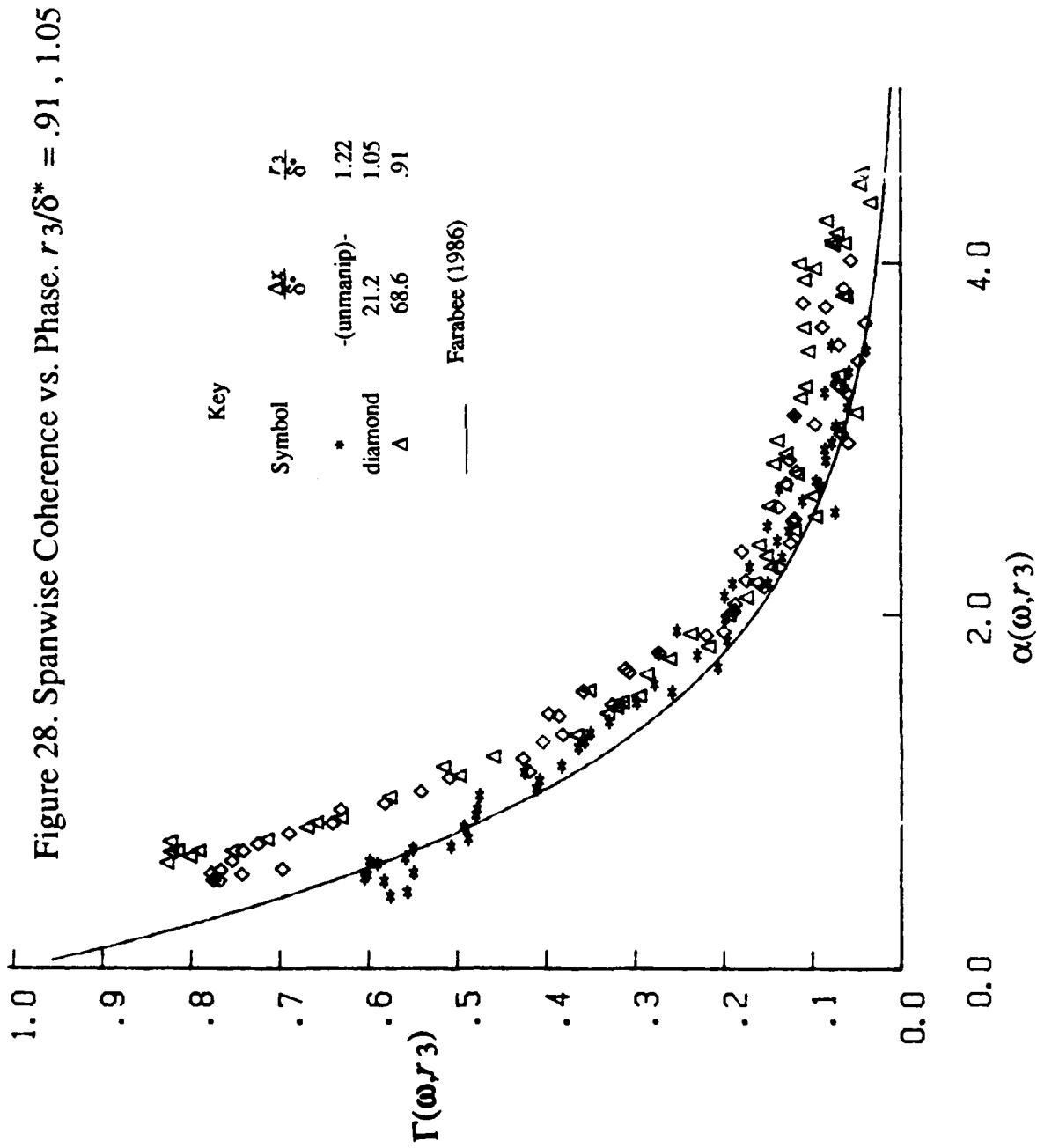
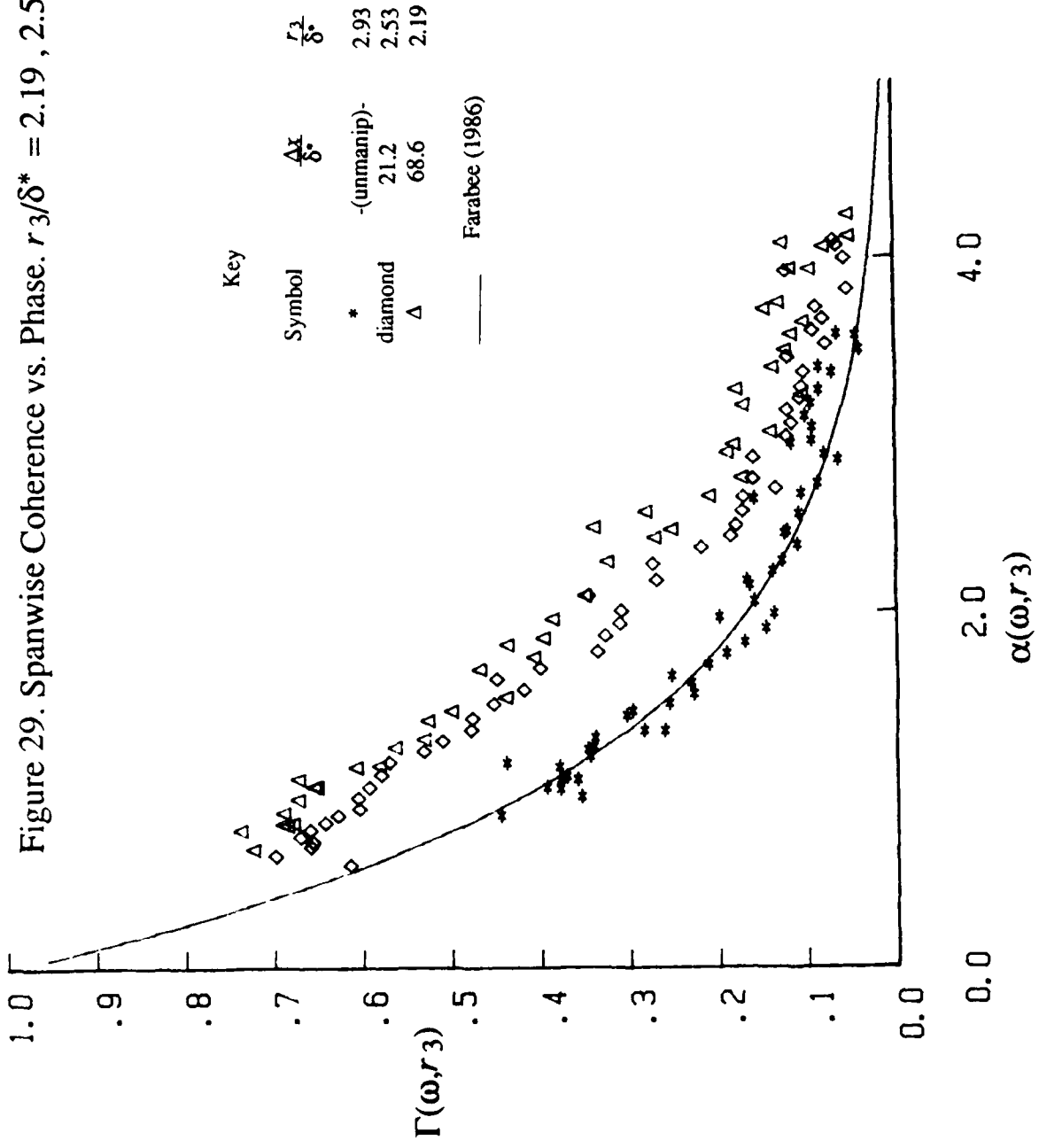


Figure 29. Spanwise Coherence vs. Phase. $r_3/\delta^* = 2.19, 2.53$



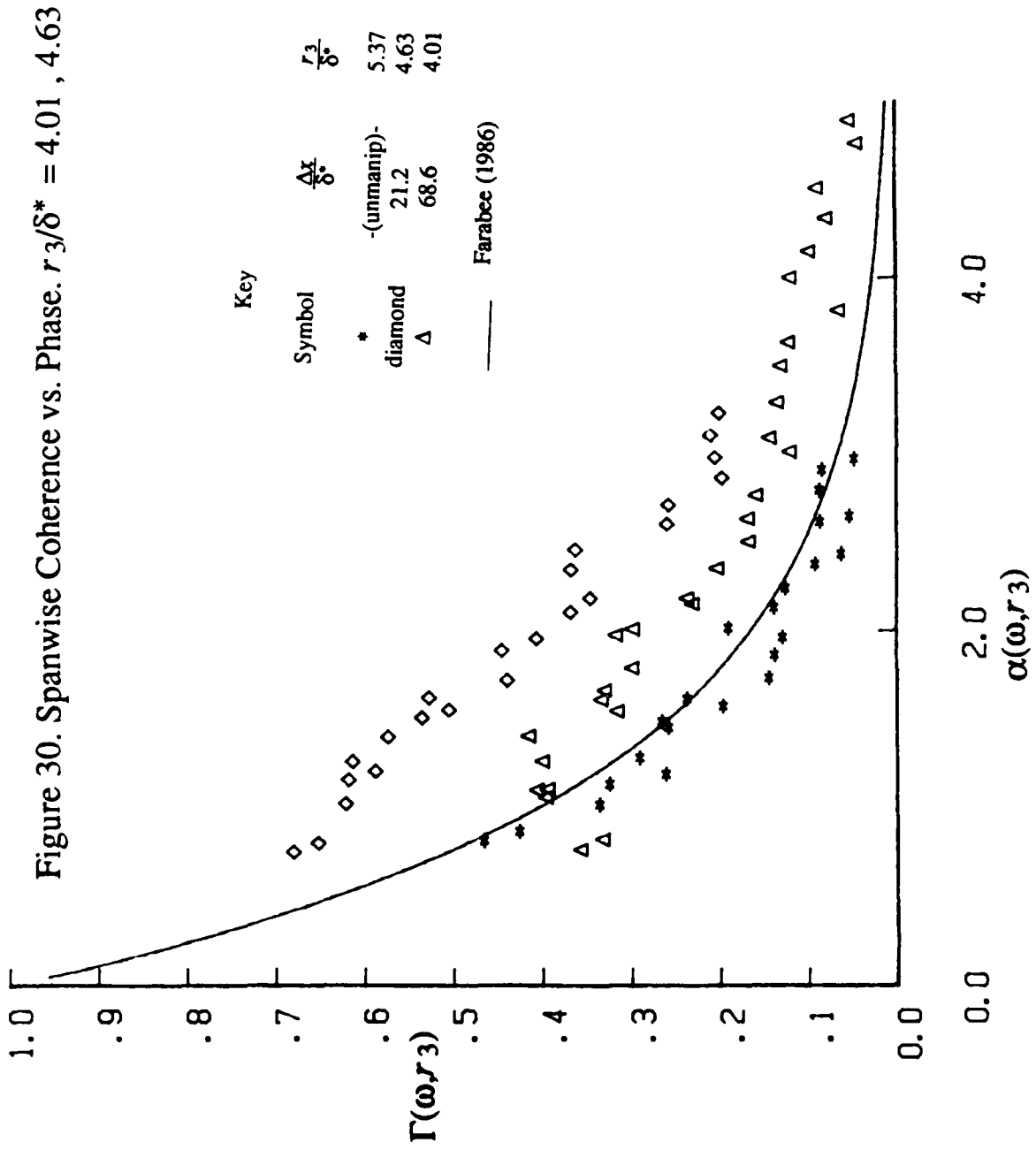
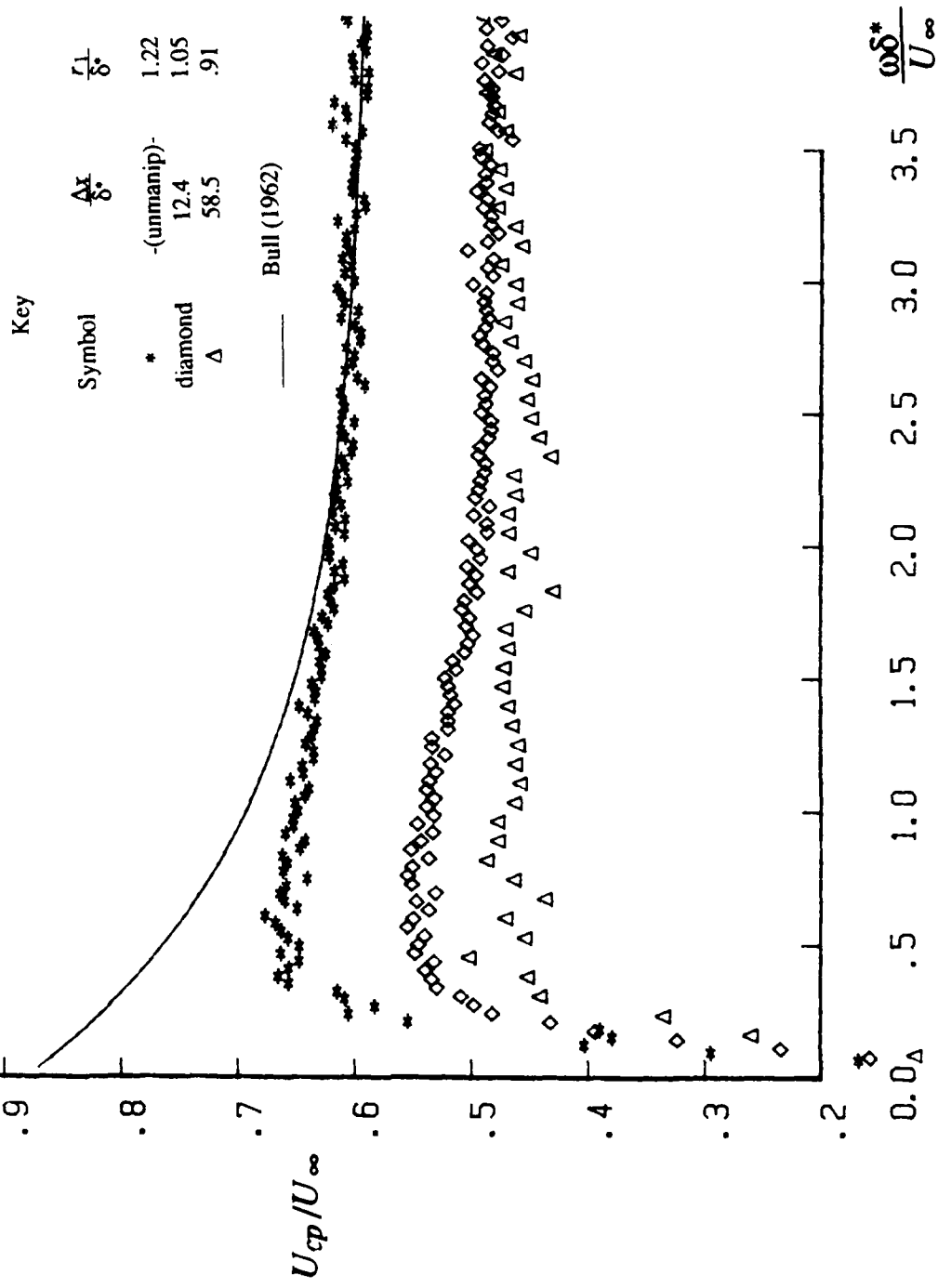


Figure 31. Convective Phase Speed vs. Strouhal Number. $r/\delta^* = .91$,

1.05



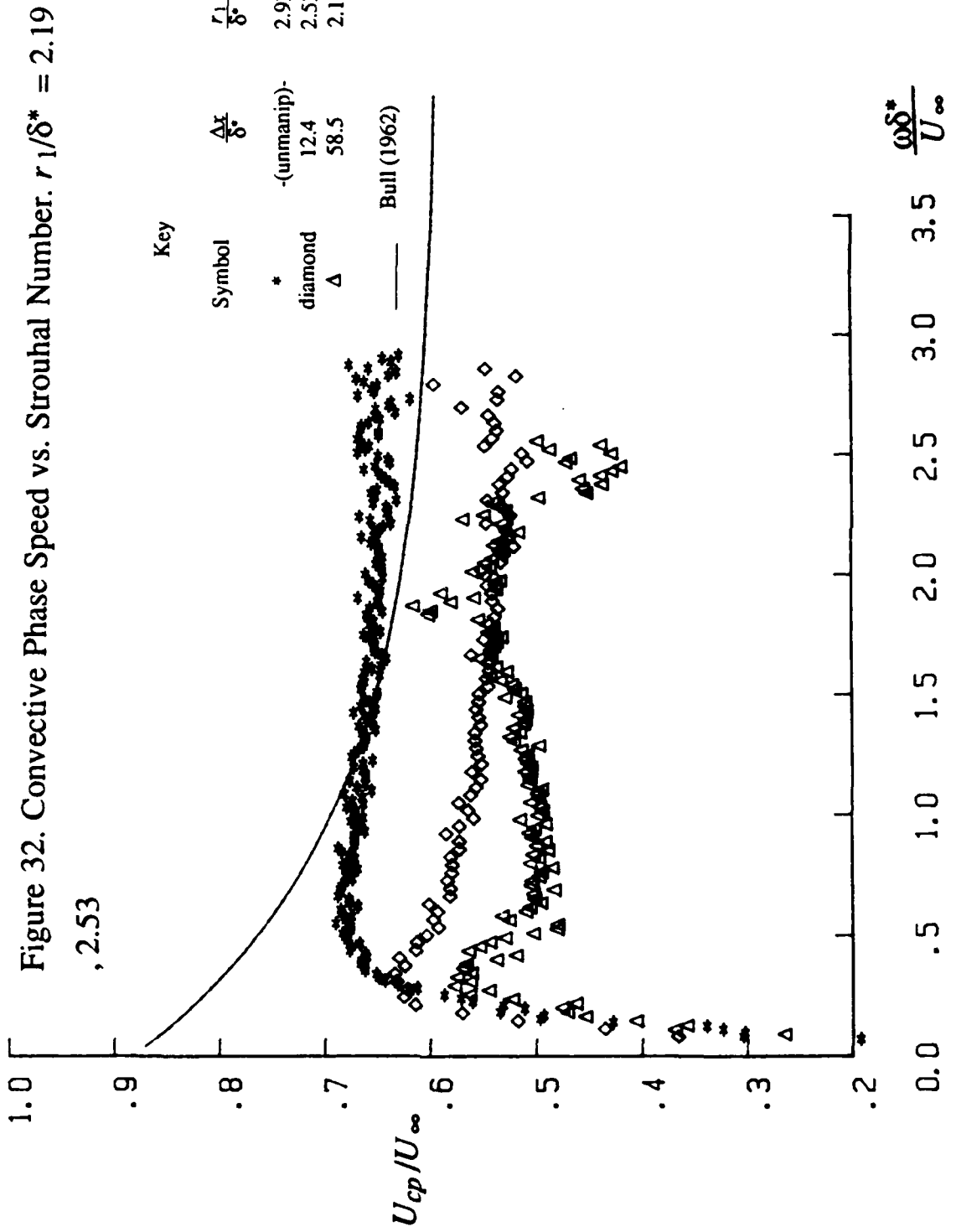


Figure 33. Convective Phase Speed vs. Strouhal Number. $r/\delta^* = 4.01$

